MATHEMATICA MONTISNIGRI
Vol XXVII (2013) 65-90

MATHEMATICAL MODELING OF NON-EQUILIBRIUM PHASE TRANSITION IN RAPIDLY HEATED THIN LIQUID FILM

V.I. MAZHUKIN[*], A.V. SHAPRANOV[*], A.A. SAMOKHIN[†], A.YU. IVOCHKIN[†]

[*] M.V. Keldysh Institute of Applied Mathematics, RAS
Moscow, Russia
Email: vim@modhef.ru
[†] A.M. Prokhorov General Physics Institute, RAS
Moscow, Russia
Email: asam40@mail.ru

Summary: In the framework of molecular dynamics the behavior of thin liquid film during its rapid homogeneous heating with rate 2-100 K/ps is studied. The initial film thickness through the *z* axis is 48 nm. The overall number of particles is 96 000 and the length of calculation area is 268 nm. In the film plane periodic boundary conditions were used with the main dimension 8x8 nm. The calculation results are presented in a form of distributions of temperature, density and particle velocity in the calculation area averaged over the film plane and also in the form of two-dimension particle density distributions in the *zx* plane in the range of heating time from 0 to 800 ps. The obtained results suggest the existence of four different regimes of film behavior depending on the heating rate: quasi-stationary regime with surface evaporation, explosive (volume) boiling, spinodal decomposition and overcritical expansion.

1 INTRODUCTION

Investigation of non-equilibrium phase transitions at rapid heating of condensed matter is of great interest both from practical and fundamental points of view. There are several unresolved problems in this area concerning in particular the peculiarities of behavior of overheated liquid phase that reaches the temperature of ultimate overheating. The most comprehensive theoretical analysis of such questions now can only been carried out with the help of mathematical modeling in the framework of molecular dynamics at which the matter behavior is considered at level of individual particles that interact with each other and with external environment.

Such approach is used in many papers in particularly in that concerning the analysis of intense laser radiation impact on condensed matter[1-5]. However in these papers the role of surface evaporation was not investigated with necessary completeness. It should be emphasized that the process of non-equilibrium phase transition considerably depends on the conditions of its realization.

In this paper the behavior of thin liquid film during its rapid homogeneous heating with the rate 2-100 K/ps is studied in the sub-nanosecond temporal range with molecular dynamics in order to find out the effect of surface evaporation on peculiarities of the process of explosive disintegration of strongly overheated film.

2010 Mathematics Subject Classification: 82C27, 82D35, 80A17.
Key words and Phrases: mathematical modeling, molecular dynamics, phase explosion, critical point, spinodal decomposition

2 STATEMENT OF THE PROBLEM

Modeling of the process of explosive boiling was carried out within the framework of molecular dynamics approach. The overall number of particles was 96 000 and the length of calculation area was 268 nm. In the film plane periodic boundary conditions were used with the main dimension 8x8 nm.

2.1 Mathematical model

The molecular dynamics approach (MD) is based on a model concept about the many-body (atomic and molecular) system, in which all particles are material points, the movement of which is described in the classic case by the Newton's equations.

The mathematical model consists of a system of differential equations, the number of which is equal to twice the number *2N* of the particles, the interatomic interaction potential $U(\vec{r}_1 \ldots \vec{r}_N)$, the specifically defined initial and boundary conditions:

$$\begin{cases} m_i \dfrac{d\vec{\upsilon}_i}{dt} = \vec{F}_i + \vec{F}_i^{ext} \\ \dfrac{d\vec{r}_i}{dt} = \vec{\upsilon}_i \end{cases}, \; i = 1 \ldots N, \tag{1}$$

where $m_i, \vec{r}_i, \vec{\upsilon}_i$ are the mass, radius-vector and velocity correspondingly; the potential energy of interaction of a system of N particles $U(\vec{r}_1 \ldots \vec{r}_N)$; $\vec{F}_i = -\dfrac{\partial U(\vec{r}_1 \ldots \vec{r}_N)}{\partial \vec{r}_i}$ - the interaction force, $\vec{F}_i^{ext}$ - the external forces.

2.2 Initial conditions

To solve the system of equations (1), it is necessary to know the coordinates and velocities $(\vec{r}_i, \vec{\upsilon}_i)\big|_{t=0}$ of all N particles at the initial time $t = 0$. During the simulation of the processes in condensed matter, the medium under consideration at the initial time can be a crystal, polycrystalline or, as in this study, liquid.

To set the initial values of the macroscopic parameters more accurately, as well as to provide a steady state in the system, we carry out a relaxation of the modeled object after setting the coordinates and velocities. To simulate liquid, it may be difficult to define the positions and velocities of the particles perfectly balanced by the kinetic and potential energies. This leads to undesired acoustic vibration. For their effective suppression, the original system of equations (1) is added by a friction term [7]:

$$\begin{cases} \dfrac{d\vec{\upsilon}_i}{dt} = \dfrac{\vec{F}_i}{m_i} - \beta \vec{\upsilon}_i \\ \dfrac{d\vec{r}_i}{dt} = \vec{\upsilon}_i \end{cases} \quad . \tag{2}$$
$$i = 1 \ldots N$$

The combined use of friction and thermostat that returns the energy to the stochastic component of the particle motion to hold the desired temperature, allows us to quickly bring the system to a steady state.

Furthermore, the pressure (tension) in the system during the relaxation may also be set to a desired level for the further simulation using a barostat.

2.3 Boundary conditions

The system (2) is a system of ordinary differential equations. Only the initial conditions are required to solve the problem. The boundary conditions are absent. However, during modeling of objects formed by a system of particles, there are often additional requirements that can be met by imposition of conditions on the boundaries of the object.

Thus, when considering the processes in a thin film with thickness H and infinite in the directions X and Y, modeling is performed in a finite computational region with dimensions $L_x \times L_y \times L_z$ along the axes, which comprises a portion of the plate $L_x \times L_y \times H$. To simulate the interaction with the part that is not included in the computational domain, periodic boundary conditions are used along the axes X and Y with the periods L_x, L_y respectively.

Periodic boundary conditions in x imply that the particles with the coordinate x in the range $0 \le x < L_x$ reproduce the particles within $kL_x \le x < (k+1)L_x$ for any integer $k \ne 0$. That is, the particle leaving the computational domain through the upper boundary is replaced by a particle with the same velocity value, but entering the computational domain through the lower boundary.

The second important aspect of periodic boundary conditions describes the force and the potential energy of interaction of particles from the boundary areas[6] $0 \le x < r_{cr}, (L_x - r_{cr}) \le x < L_x$ where r_{cr} is the cutoff radius of the potential (it is assumed that the forces acting at the distances $r > r_{cr}$ can be ignored). Interaction of the particle i, with the coordinate x_i being in the range of $(L_x - r_{cr}) \le x_i < L_x$ with the particles outside the computational domain, $L_x \le x'_j < (L_x + r_{cr})$, is modeled using the particles from the range of $0 \le x_j < r_{cr}$ from the computational domain, which radius-vectors are corrected in the following way during the computation of the force $\vec{F}_{ij} = \vec{F}_{(\ldots \vec{r}'_j \ldots)}(\vec{r}_i)$:

$$\vec{r}'_j = \vec{r}_j + \vec{e}_x L_x ,$$

where $\vec{e}_x$ is the unit vector of the axis X.

Obviously, all above is equally applied to the periodic boundary conditions along the coordinate axis Y.

The question of the error introduced by the periodic boundary conditions is associated with the distortion introduced in the damping of the phonon modes in the crystal. Obviously, increasing the distance between the boundaries reduces the effect on the spectrum of the phonon modes.

2.4 Interaction potential

As the interaction potential we used the potential of the “embedded atom” (Embedded Atom

Model - EAM)[7-8], which made a good account of itself for the materials with a metallic bond. The contribution to the energy of randomly arranged nuclei from the interaction with the electrons, according to the quantum mechanical density functional theory, can be written as a unique functional of the total electron density (embedded functional). In this case, the total electron density in the metal is a linear superposition of the contributions of individual atoms, and the electron density that is created by a single atom is spherically symmetric. Thus, the total energy of the system consists of two components - the energy of the pair interaction of atoms and the interaction energy of each atom with an electron density produced by other atoms:

$$U(\vec{r}_1 \ldots \vec{r}_N) = \frac{1}{2} \sum_{\substack{i,j=1 \\ i \neq j}}^{N} \varphi(r_{ij}) + \sum_{i=1}^{N} f(\rho_i),$$

where $\varphi(r_{ij})$ is the pair potential, $f(\rho_i)$ is the embedded functional of *i*-th atom, ρ_i is the total electron density for the *i*-th atom, produced by spherically-symmetric functions of single electron density $n(r_{ij})$ of other atoms.

In this problem, we used as the potential one of the semi-empirical "embedded-atom" potentials given in [9]. A polynomial relationship was used in [9] as the pair part:

$$\varphi(r) = \begin{cases} 0, & r \geq r_c \\ \left(\dfrac{1}{a_1 r^2} - a_2 \right) \left(a_1 r^2 - a_1 r_c^2 \right)^{10} \left[\left(a_1 r^2 - a_1 r_c^2 \right)^6 + a_3 \left(a_1 r^2 \right)^6 \right], & r < r_c \end{cases}$$

Analytical expressions were used for the embedded function and single-electron density:

$$f(\rho) = \frac{b_1 \rho \cdot \left[b_2 + (b_3 + \rho)^2 \right]}{1 + b_4 \rho}, \quad n(r) = \begin{cases} 0, & r \geq r_c \\ \dfrac{c_1 \cdot \left(r^2 - r_c^2 \right)^2}{1 + \left(c_2 r^2 \right)^3}, & r < r_c \end{cases}$$

where $r_c = 0.6875$ nm is the cut-off radius of the potential, a_1 - a_3, b_1 - b_4, c_1 - c_2 are the fitting constants.

The parametrization of the potential was carried out based on mechanical characteristics of aluminum. To estimate its applicability to the solution of thermal problems, the calculation results obtained with it, were compared with the actual thermal characteristics, such as melting point, specific heat of fusion, heat capacity, thermal expansion coefficient[10-11].

3. COMPUTATIONAL ALGORITHM

The essential feature of the molecular dynamics simulation is the need to calculate the trajectories of a huge number of particles. So for a cube of aluminum (face-centered lattice constant a = 0.405 nm) with an edge $L = 0.1$ μm the estimate of the number of particles is $N = 4L^3/a^3 \approx 6 \cdot 10^7$.

3.1 Differential approximation

As the best compromise between the computational efficiency and requirements of accuracy and stability, Verlet algorithm is widely used in molecular dynamics simulation[12] in its most convenient, so-called velocity form. The further proposed its modification comprises, unlike the original, additional friction. For the system of equations (2) with viscosity one can write the following finite-difference approximation:

$$\frac{\vec{\upsilon}^{k+1}-\vec{\upsilon}^{k}}{\Delta t}=\frac{\vec{a}^{k}+\vec{a}^{k+1}}{2}-\beta\frac{\vec{\upsilon}^{k+1}+\vec{\upsilon}^{k}}{2}\;\Rightarrow\;\vec{\upsilon}^{k+1}\left(1+\frac{\beta\Delta t}{2}\right)=\overbrace{\vec{\upsilon}^{k}\left(1-\frac{\beta\Delta t}{2}\right)}^{\vec{\upsilon}_{*}^{k+1/2}}+\frac{\vec{a}^{k}\Delta t}{2}+\frac{\vec{a}^{k+1}\Delta t}{2}$$

$$\frac{\vec{r}^{k+1}-\vec{r}^{k}}{\Delta t}=\vec{\upsilon}_{*}^{k+1/2}\;\Rightarrow\;\vec{r}^{k+1}=\vec{r}^{k}+\vec{\upsilon}_{*}^{k+1/2}\Delta t=\vec{r}^{k}+\vec{\upsilon}^{k}\Delta t+\frac{(\vec{a}^{k}-\beta\vec{\upsilon}^{k})\Delta t^{2}}{2}$$

Here upper index k is the number of time step, $\vec{a}=\vec{F}/m$ is the acceleration, index *i* (part number) is omitted. Determination of intermediate velocity in the half-integer moment of time:

$$\vec{\upsilon}_{*}^{k+1/2}=\vec{\upsilon}^{k}\left(1-\frac{\beta\Delta t}{2}\right)+\frac{\vec{a}^{k}\Delta t}{2}$$

is equivalent to the differential approximation:

$$\frac{\vec{\upsilon}_{*}^{k+1/2}-\vec{\upsilon}^{k}}{\Delta t/2}=\vec{a}^{k}-\beta\vec{\upsilon}^{k}.$$

As a result, the computational algorithm of Verlet in the velocity form for the system (2) with the viscosity is formulated as follows. Assuming that all the relevant values are known at the time t_k, the transition to the next point in time $t_{k+1}=t_k+\Delta t$ is calculated as:

$$\begin{aligned}
&\vec{\upsilon}_{*}^{k+1/2}=\vec{\upsilon}^{k}\left(1-\frac{\beta\Delta t}{2}\right)+\frac{\vec{a}^{k}\Delta t}{2}\\
&\vec{r}^{k+1}=\vec{r}^{k}+\vec{\upsilon}_{*}^{k+1/2}\Delta t\\
&\vec{a}^{k+1}=-\frac{\mathrm{grad}(U^{k+1})}{m}\\
&\vec{\upsilon}^{k+1}=\frac{\vec{\upsilon}_{*}^{k+1/2}+\dfrac{\vec{a}^{k+1}\Delta t}{2}}{1+\dfrac{\beta\Delta t}{2}}
\end{aligned}\qquad(3)$$

The scheme of Verlet is not conservative in the sense of the exact realization of the law of conservation of energy in the differential form. However, statistically, for a particle system this law holds quite well.

3.2 Calculation of macroscopic values

Local thermodynamic equilibrium is quickly established during the molecular dynamics modeling of condensed matter. Thus, the typical time of the local equilibrium distribution of aluminum in the crystal is a few picoseconds. Accordingly, by using the averaging procedure[6] we determine the basic thermodynamic quantities - the pressure (stress in the crystal) and temperature as well as the velocity and density. For the purpose of the spatial averaging, the entire set of atoms under consideration was divided into cells, where the averaging of stochastic components was performed.

4. RESULTS AND DISCUSSION

4.1 Slow heating (stationary regime)

It is obvious that at a sufficiently slow heating the film can evolve from the initial state to a stationary evaporation regime with the balance between of supplied energy and the evaporation energy loss that depends in particular on the film dimensions.

For such a regime with the heating rate 2 K/ps the calculation results are presented in Fig. 1-8. In Fig. 1a-1b the initial distributions of temperature, density and particle velocity at the $t = 0$ when the film is in equilibrium with its saturated vapor at temperature 6400 K are presented. It is clearly seen from Fig. 1 that the density value of saturated vapor is approximately 0.04 g/cm^3 as compared with film density 1.3 g/cm^3. The initial film thickness was 48 nm, the length of the area with saturated vapor was 22 nm from each side.

After the boundaries are opened and heating is started at $t > 0$ the vapor density and its temperature decrease and become non-homogeneous due to expansion (Fig. 2, $t = 10$ ps) and the film surface temperature also begins to decrease due to evaporation (Fig. 2, 5-6). At first a small decrease of bulk temperature is observed which is seemingly induced by additional film expansion due to decrease of external pressure that becomes lower than the saturation pressure for given surface temperature. Vapor particles velocity at the film boundary initially has the low value that corresponds to the regime of expansion of initial layer of saturated vapor. With time the particle velocity amplitude at the film surface increases that is typical for beginning of intense evaporation.

As a result a quasi-stationary convex temperature profile and corresponding (according to equation of state) concave density profile are formed (Fig. 5-6).

Film temperature maximum at the time moment t > 200 ps sets up at level ~ 6800 K ~ 0.9 T_c, where T_C ~ 7600 K – critical temperature, and practically does not change through subsequent 500 ps as it is seen from Figure 5a-6a.

Fluctuations of density and temperature in the condensed phase are relatively small. It should be mentioned that the energy transfer to the particles is realized only when the density is greater than 0.3 of current spatial maximum density.

Parameters of such quasi-stationary regime of evaporation in the simplest approximation can be analytically determined supposing quadratic distribution of temperature over the film with maximum in the central part. Results of such analytical estimation will be presented elsewhere.

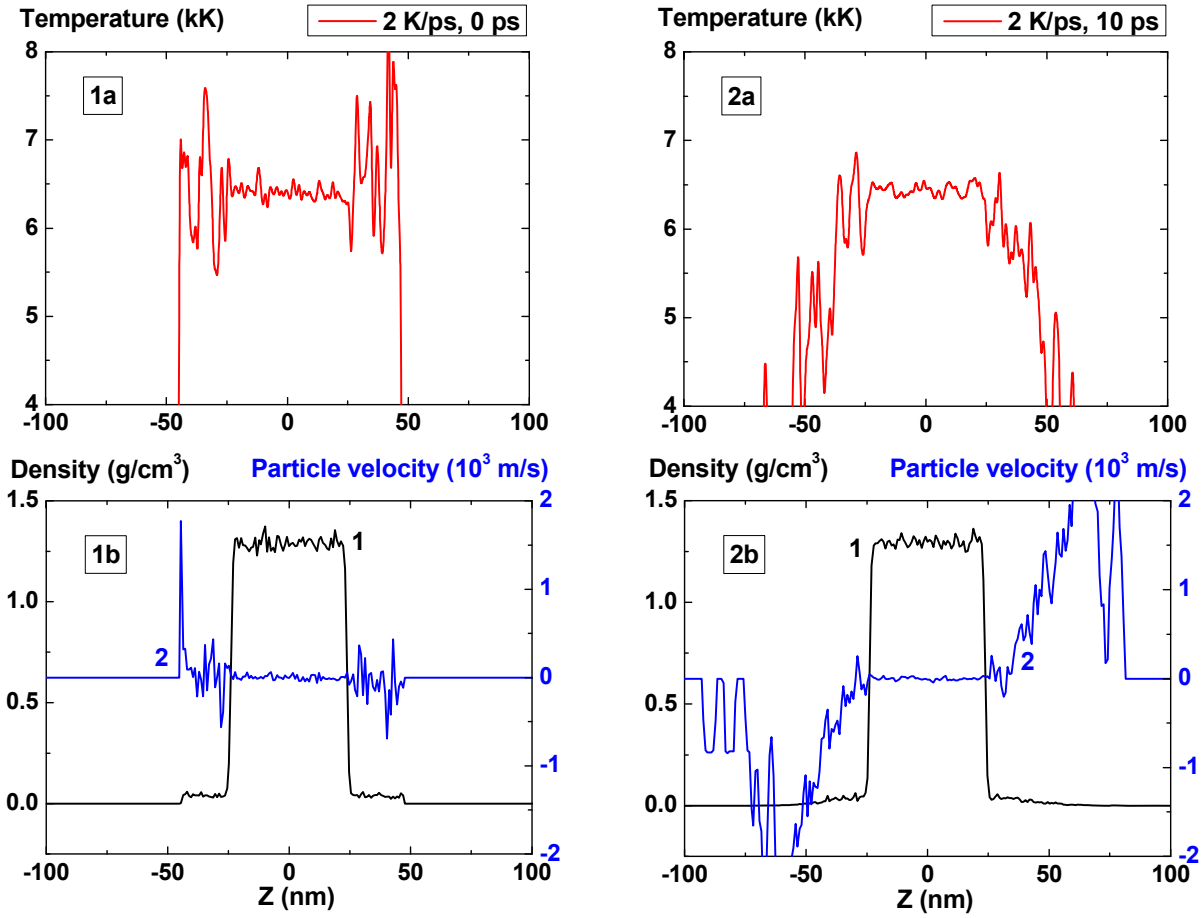

Figures 1-2: Spatial distributions of temperature (1a-2a), density (1b-2b, curve 1) and particle velocity (1b-2b, curve 2) through the film at moments 0, 10 ps during heating with 2 K/ps rate

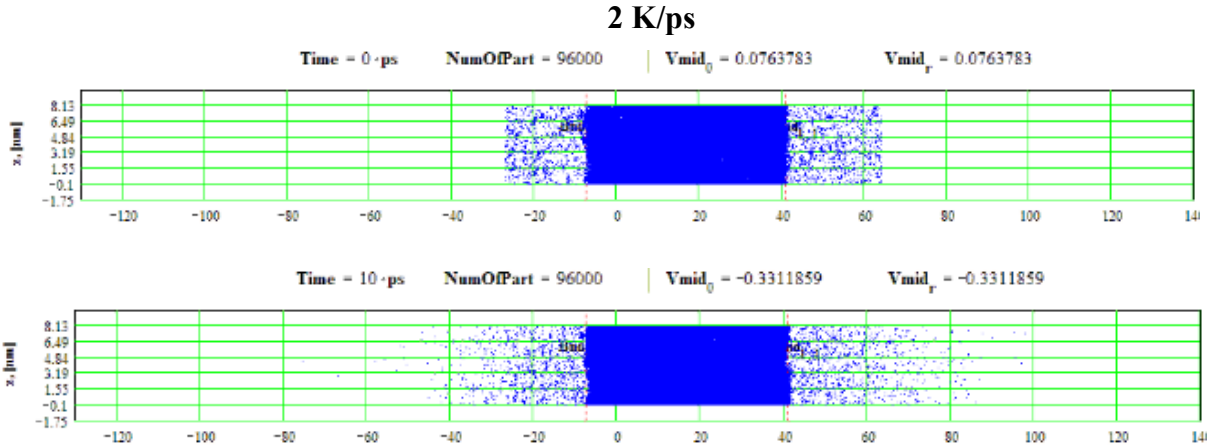

Figures 3-4: Spatial distributions of film particles at time moments 0, 10 ps during heating with 2 K/ps rate

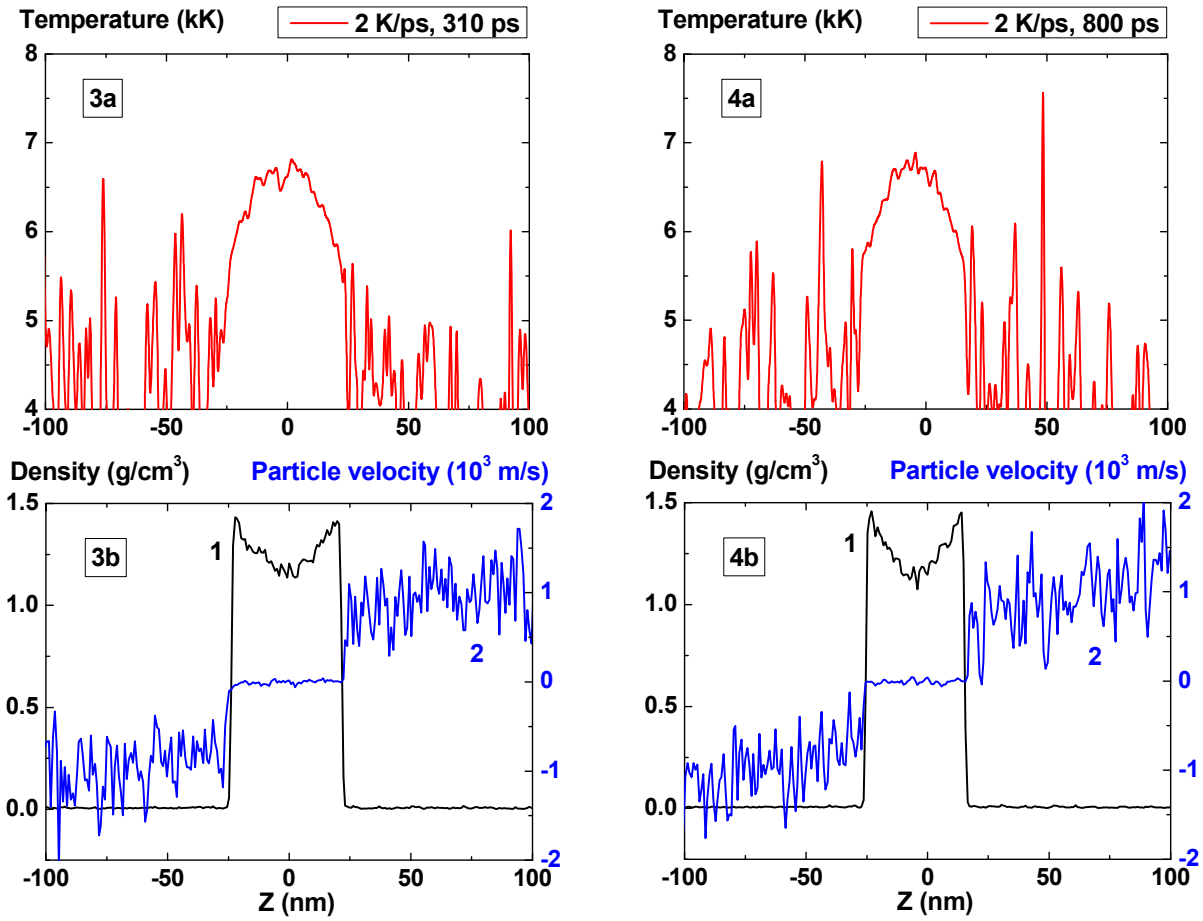

Figures 5-6: Spatial distributions of temperature (5a-6a), density (5b-6b, curve 1) and particle velocity (5b-6b, curve 2) through the film at moments 310, 800 ps during heating with 2 K/ps rate

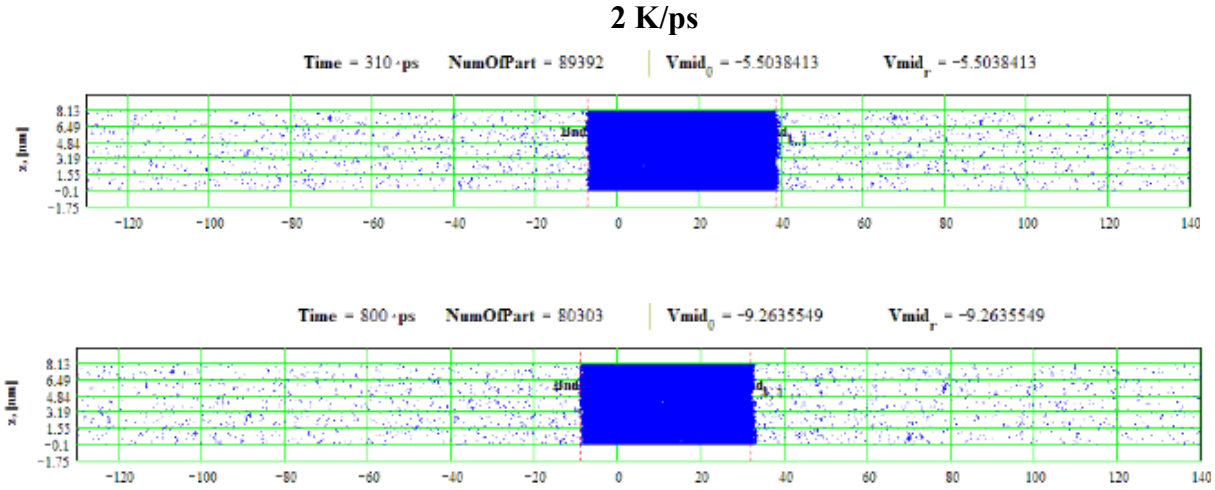

Figures 7-8: Spatial distributions of film particles at time moments 310, 800 ps during heating with 2 K/ps rate

The considered case of quasi-stationary state has limited existence time not only due

to the limited film thickness and its evaporation. The film is in an overheated metastable state which temperature is greater than the temperature of phase equilibrium (binodal) for given pressure and density is lower than equilibrium value. In such state there is a finite possibility of formation of growing hetero-phase fluctuations that emerge due to spontaneous homogeneous nucleation of new (vapor) phase seeds. The waiting time of such fluctuations rapidly decreases when T_m approaches the temperature of ultimate overheating (spinodal)[13].

4.2 Explosive boiling regime

At the heating rate of 4 K/ps from the same initial state up to the time moment t = 240 ps (Fig. 9, 11) the film behavior differs but slightly from the previous case and the achieved temperature maximum is about 7000 K that is ~ 200 K higher than the previous value.

Than, however, instead of continuation of quasi-stationary regime the process of explosive boiling i.e. rapid local decrease of density and formation of vapor cavity inside the film localized near the maximum of temperature profile (Figure 10, 12, 13-16) starts. The cavity formation process is accompanied by local decrease of temperature at the area of its previous maximum.

The maximum temperature value at which the process of explosive boiling starts exceeds its value in quasi-stationary regime only by a small amount $T \sim 10^{-2}\ T_c$ that indicates sharp enough temperature limit of the start of the explosive boiling process in nanosecond range of its anticipation[13].

The sharp temperature dependence of explosion anticipation time is already known for a long time (V.P. Skripov). In the framework of molecular dynamics with usage of NPT ensemble this dependence was studied for example in[14]. However such approach doesn't give the possibility to observe the peculiarities of the decomposition process connected with the existence of surface evaporation which plays a considerable role in this case.

The increase of density fluctuations in comparison with previous regime is seen even at Fig. 9 (t = 240 ps) and at the time moment t = 300 ps (Fig. 13) the minimum value of density in the film center approaches the critical value of density 0.47 g/cm^3. At the same time the temperature decrease in the area of temperature maximum due to beginning of process of evaporation into the cavity is already seen. It should be noted that this local minimum can be connected with the relative increase of heat capacity of condensed phase C_p when temperature approaches the limit of ultimate overheating.

The further cavity growth and fragments movement are determined by the vapor pressure difference between the fragments and outside them. The vapor density inside the cavity is noticeably higher than the density outside the fragments as it is seen at the density distribution curve at Fig. 14.

The temporal dependence of fragments velocity after t = 300 ps is shown in Fig. 17. The fragments velocities differ slightly due to difference in its mass (or thickness h). More massive right fragment with thickness h_2 = 25 (at t = 450 ps) nm moves slowly than left with h_1 = 21 nm (at t = 450 ps). According to the momentum conservation law the values of velocities and fragments thicknesses are related by $v_1h_1 = v_2h_2$ in the center mass system which coincides with the laboratory system.

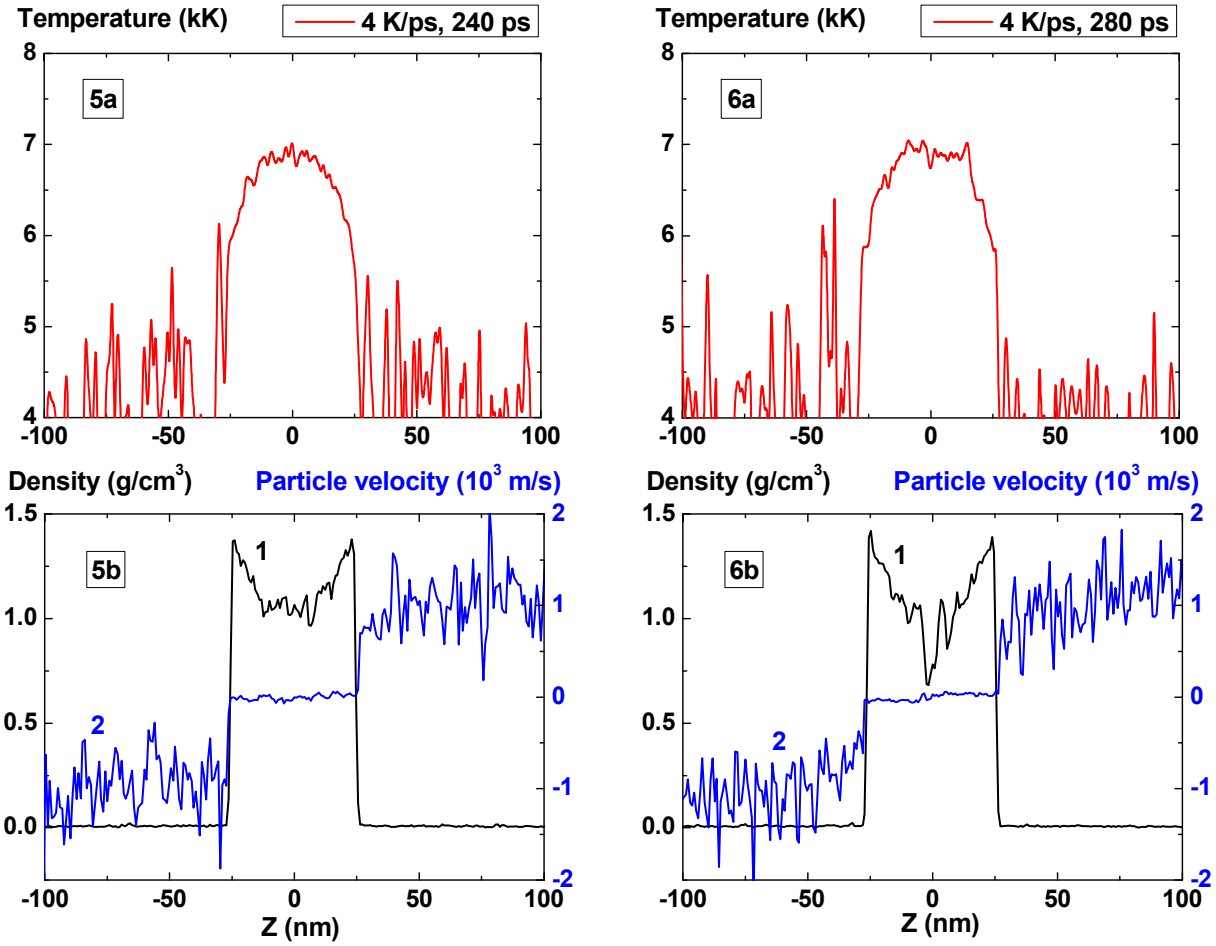

Figures 9-10: Spatial distributions of temperature (9a-10a), density (9b-10b, curve 1) and particle velocity (9b-10b, curve 2) through the film at moments 240, 280 ps during heating with 4 K/ps rate

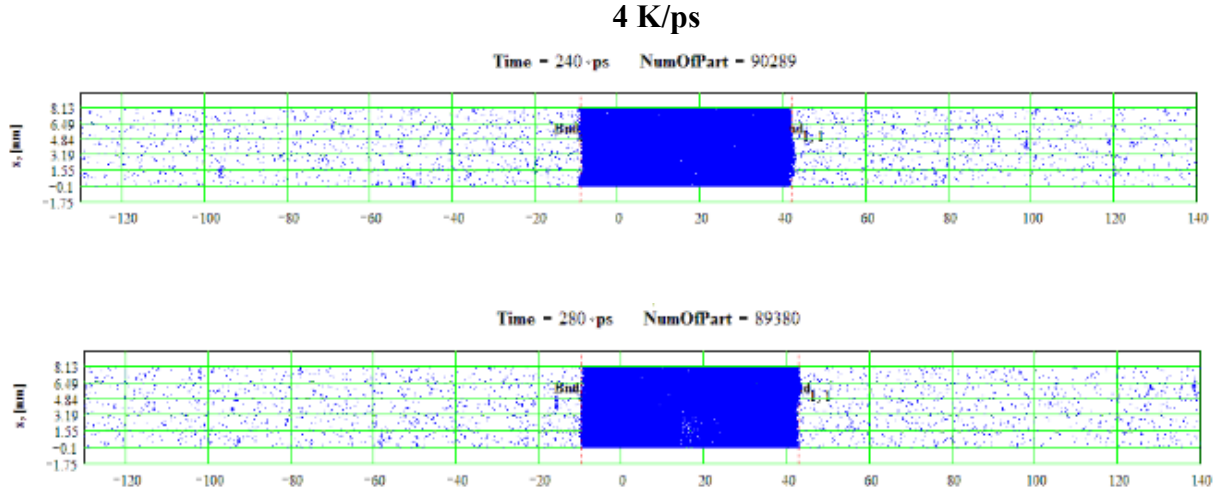

Figures 11-12: Spatial distributions of film particles at time moments 240, 280 ps during heating with 4 K/ps rate

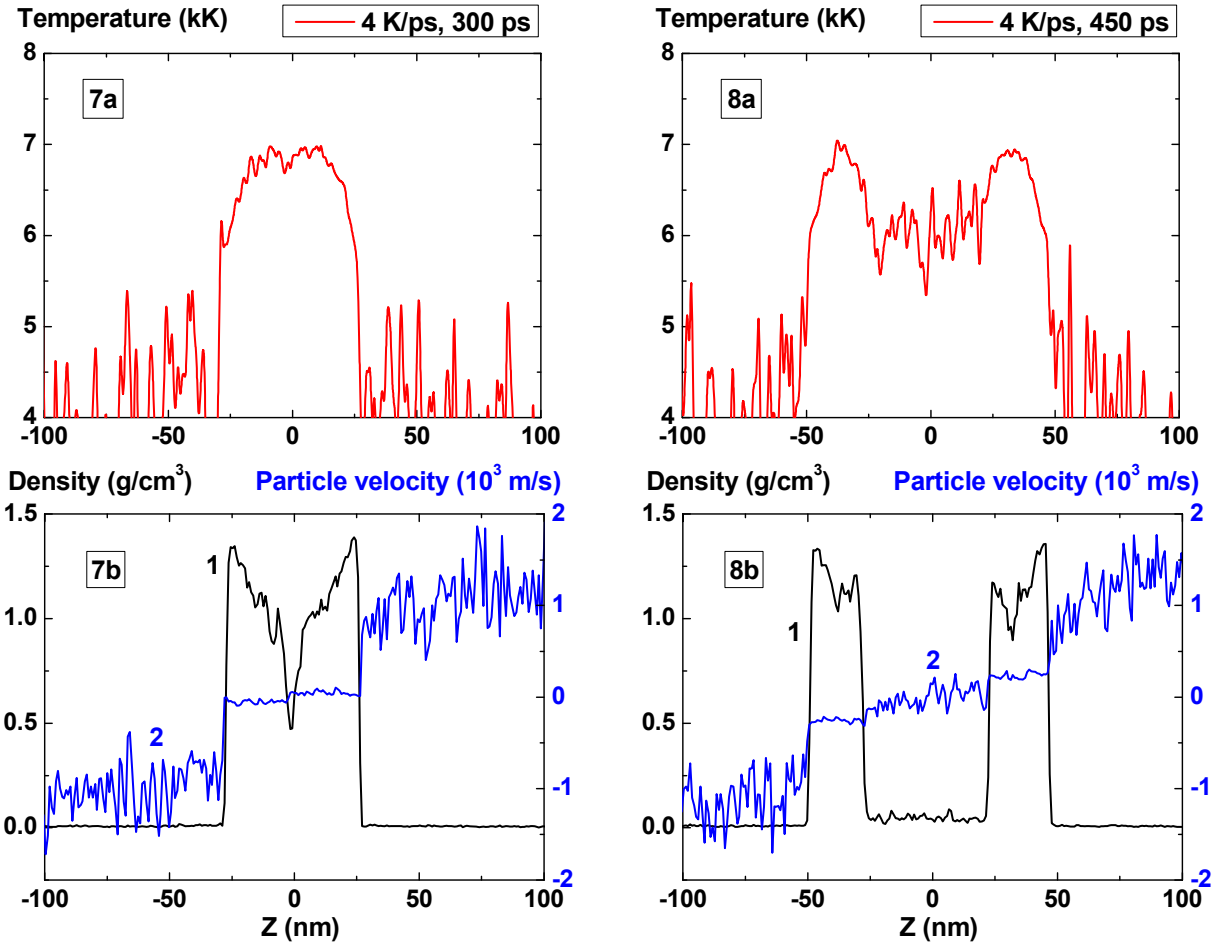

Figures: 13-14 Spatial distributions of temperature (13a-14a), density (13b-14b, curve 1) and particle velocity (13b-14b, curve 2) through the film at moments 300, 450 ps during heating with 4 K/ps rate

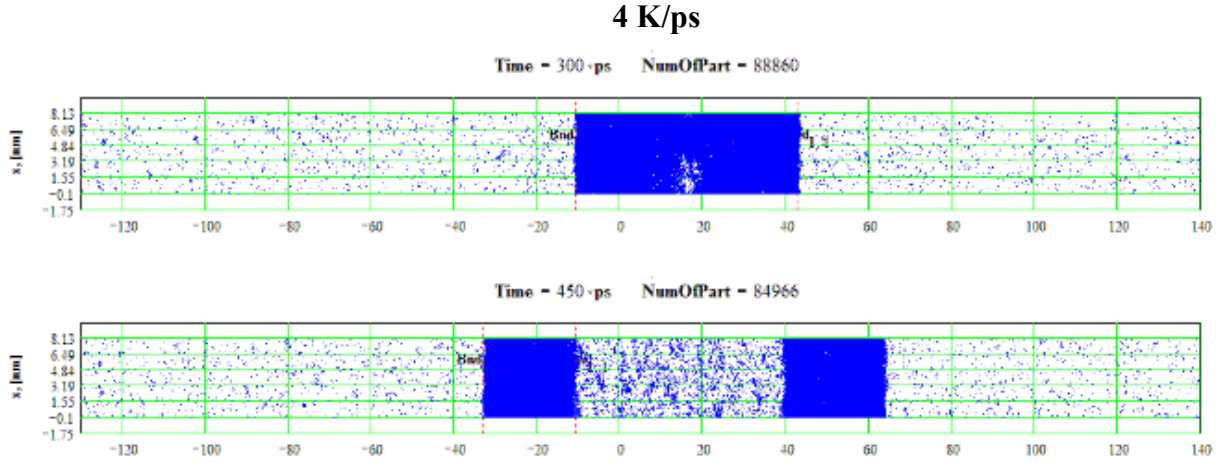

Figures 15-16: Spatial distributions of film particles at time moments 300, 450 ps during heating with 4 K/ps rate

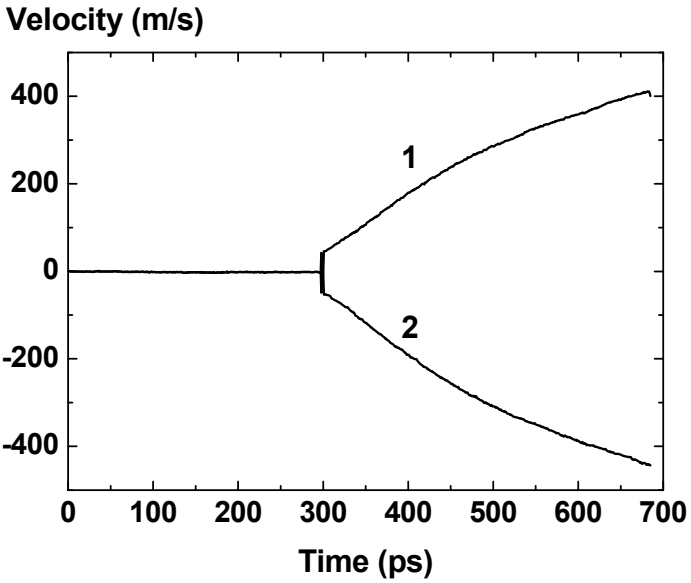

Figure 17: Velocity vs time for right (1) and left (2) fragments of the expanding film for hearting rate 4K/ps

The behavior of fragments velocity (acceleration) at the initial moment of cavity formation contains information about value of pressure that develops in this explosive boiling process. According to the Newton's law there is relation between the fragment acceleration and the resulting pressure P acting on it which is equal to the pressure difference between the inner and outer fragment's border $P = a\rho h$, where a, ρ, h – fragment acceleration, thickness, and density correspondingly. The quantitative determination of initial (maximal) acceleration using numerical data on fragments movement is difficult due to low precision of such procedure.

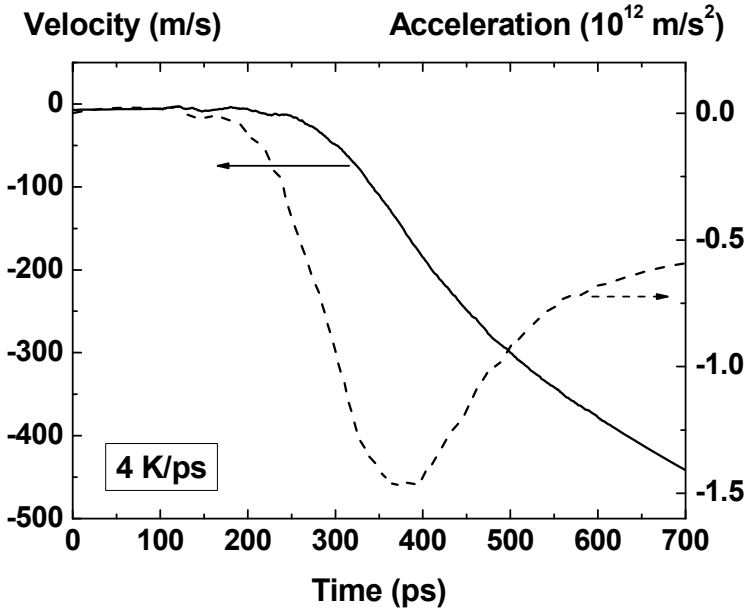

Figure 18: Velocity (solid line) and acceleration (dashed line) vs time of left (2) fragment at hearting rate 4K/ps

In Fig. 18 the behavior of displacement, velocity and acceleration of outer boundary of left fragment are shown. The maximum absolute value of acceleration is ~ $1.5 \cdot 10^{12}$ m/s^2 that corresponds to the maximum pressure $P_m = a\rho h + P_0 \sim 500$ atm, where $\rho = 1.2$ g/cm^3, $h = 23$ nm, $P_0 \sim 100$ atm – pressure at the outer boarder of the fragment. The pressure value obtained in MD calculation also leads to significant space-temporal fluctuations of this value and its averaged value is also about 500 atm that is ~ 0.35 P_c, where P_c ~ 1420 atm – critical pressure. The saturation pressure for the film temperature $T = 7000$ K is about 840 atm that is greater than the obtained maximum pressure value.

Acceleration rise time (~ 100 ps) is determined by the pressure growth in the forming cavity due to phase explosion. This cavity formation process in the given time range is shown in 2D in Fig. 15-16. It should be noted that the pressure rise time during phase explosion is not much greater than the time of the sound round-trip over the fragment, i.e. hyper-sound vibrations can be induced in the expanding fragments as a result of such process.

Explosive boiling is a strong non-equilibrium process when fluctuations rapidly grow in metastable (non-equilibrium) state of overheated liquid. This process is stochastical in nature and its behavior is not determined only by average values of thermo-dynamical parameters. According to this fact for the same heating rate 4 K/ps due to fluctuation differences in initial state not one but two cavities can be formed as a result of phase explosion divided approximately in the middle by a thin (~ 5 nm) film of condensed phase. This difference is seen at 2D images of density distribution (Fig. 19-20)

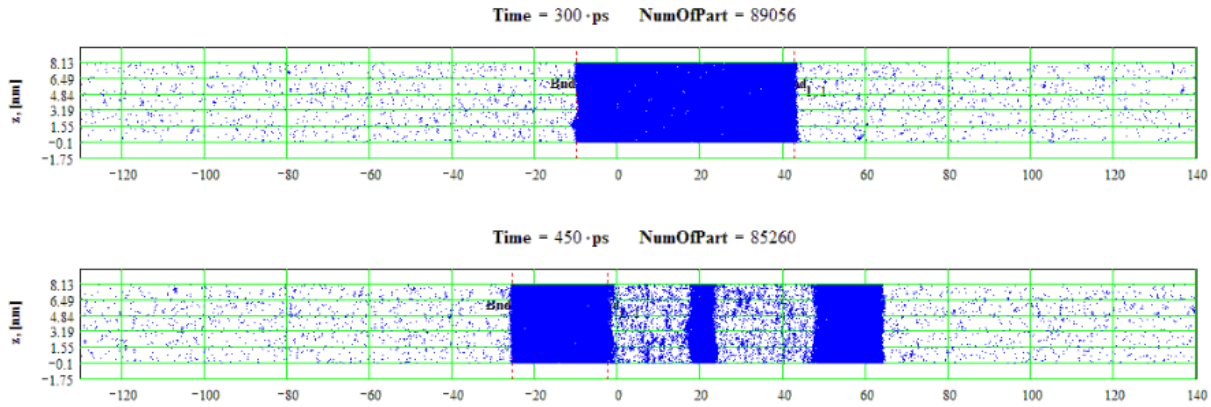

Figures 19-20: Spatial distributions of film particles at time moments 300, 450 ps during heating with 4 K/ps rate (another ititial conditions)

4.3 Rapid heating and near-critical expansion regime

Increase of the heating rate up to 8 K/ps leads to a more complex multiply connected density distribution in the expanding film (Fig. 21-30). The moment of the start of film disintegration (180 ps) at $T = 7000$ K when fluctuated density approaches value 0.7 g/cm^3 is shifted to more earlier times in comparison with the start of the film decomposition onto two fragments (300 ps for the heating rate 4 K/ps).

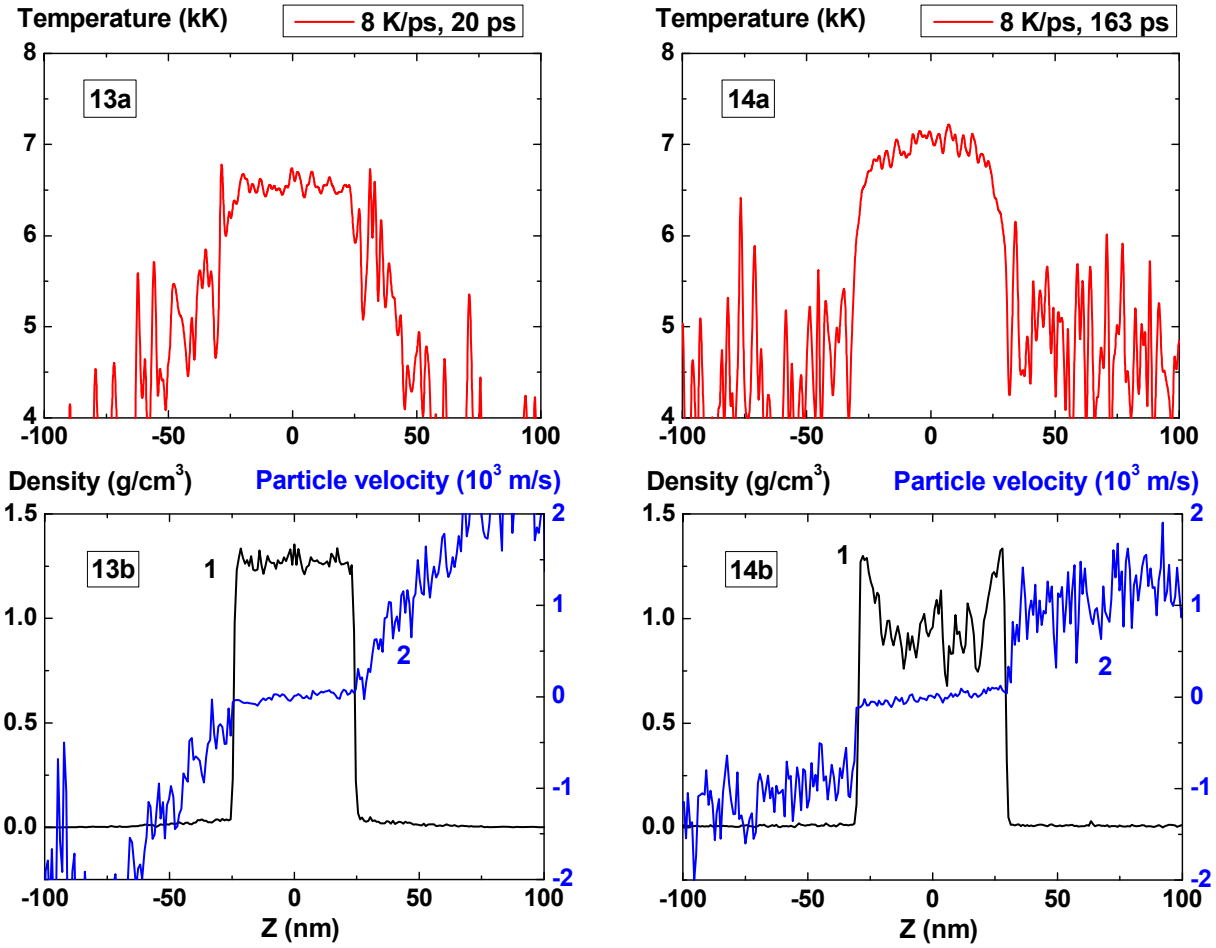

Figures 21-22: Spatial distributions of temperature (21a-22a), density (21b-22b, curve 1) and particle velocity (21b-22b, curve 2) through the film at moments 20, 163 ps during heating with 8 K/ps rate

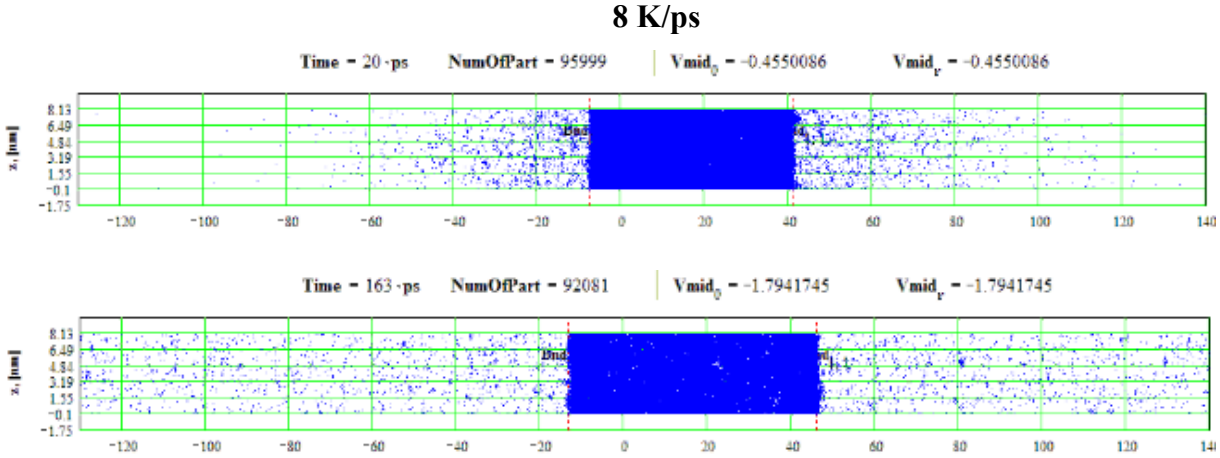

Figures 23-24: Spatial distributions of film particles at time moments 20, 163 ps during heating with 8 K/ps rate

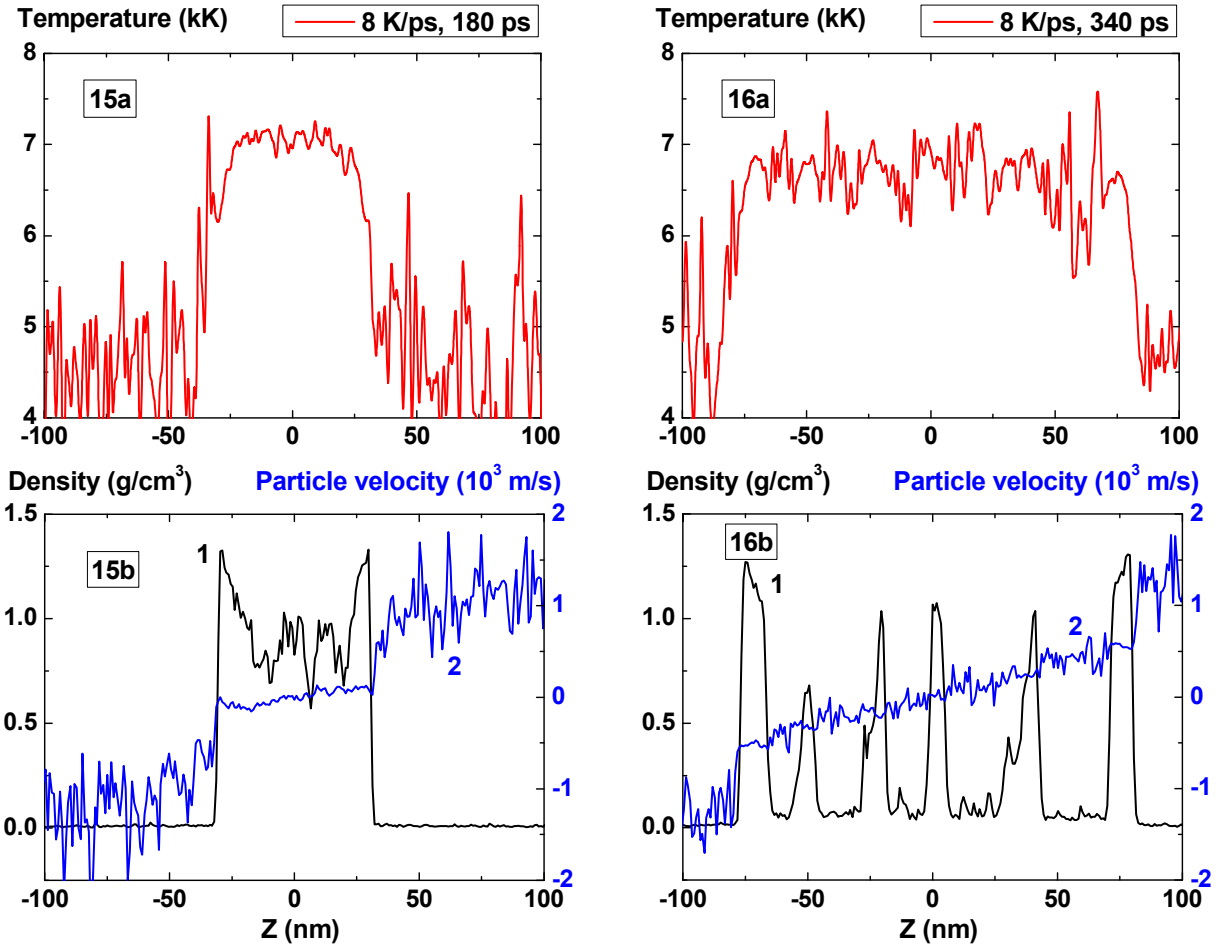

Figures 25-26: Spatial distributions of temperature (25a-26a), density (25b-26b, curve 1) and particle velocity (25b-26b, curve 2) through the film at moments 180, 340 ps during heating with 8 K/ps rate

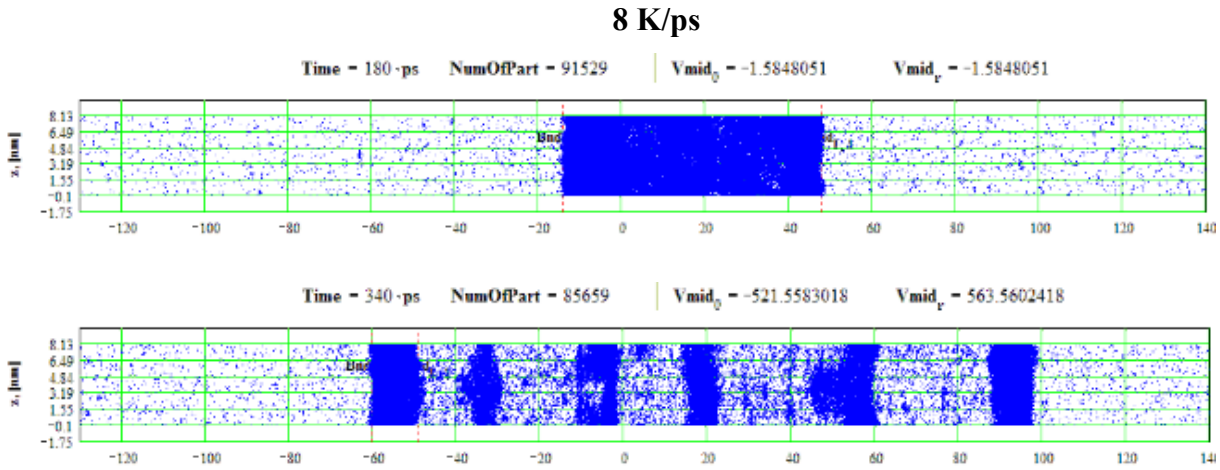

Figures 27-28: Spatial distributions of film particles at time moments 180, 340 ps during heating with 8 K/ps rate

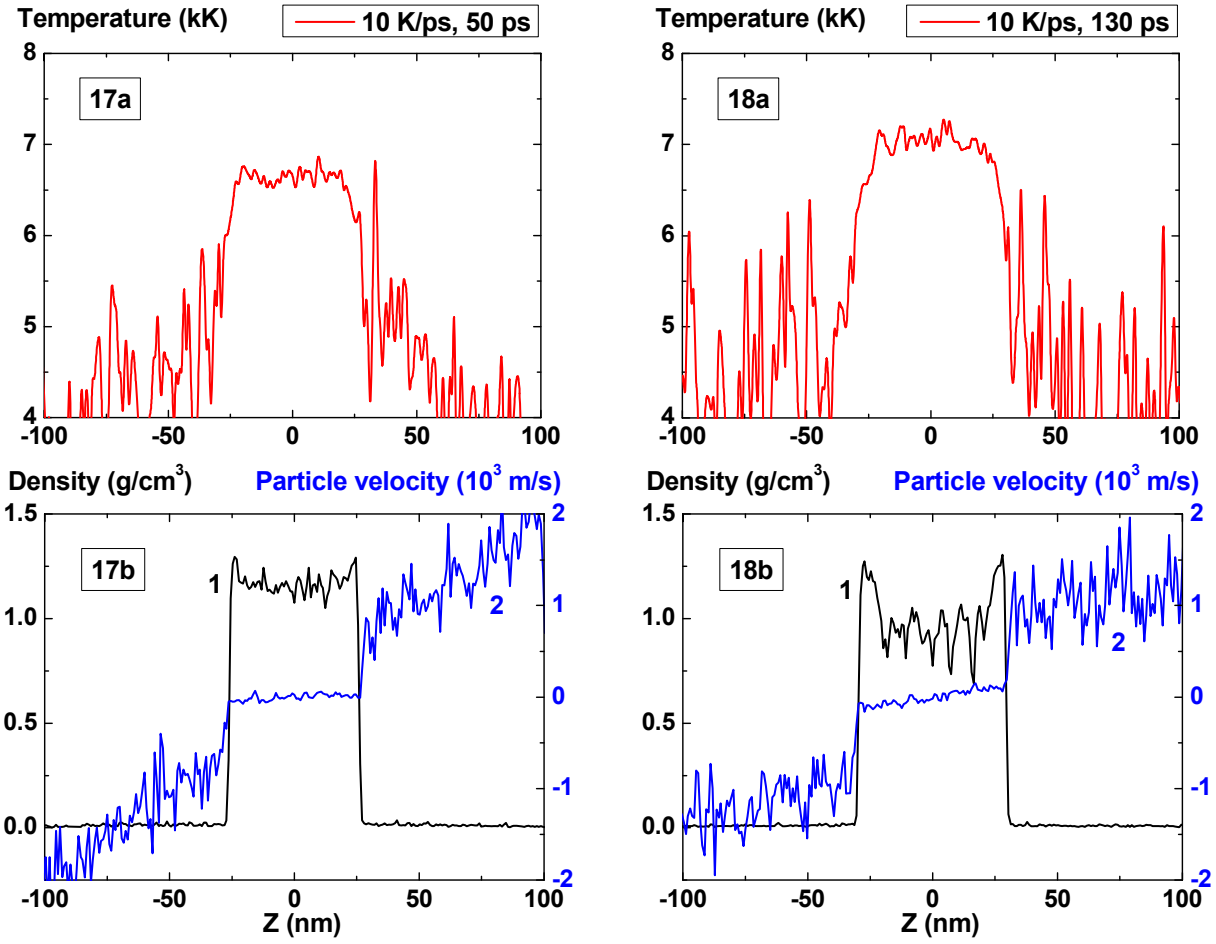

Figures 29-30: Spatial distributions of temperature (29a-30a), density (29b-30b, curve 1) and particle velocity (29b-30b, curve 2) through the film at moments 50, 130 ps during heating with 10 K/ps rate

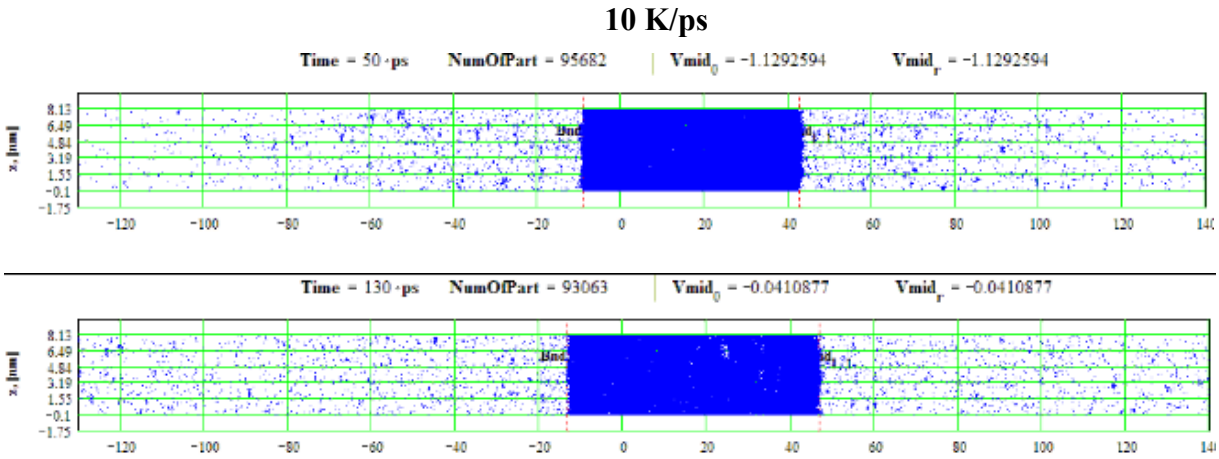

Figures 31-32: Spatial distributions of film particles at time moments 50, 130 ps during heating with 10 K/ps rate

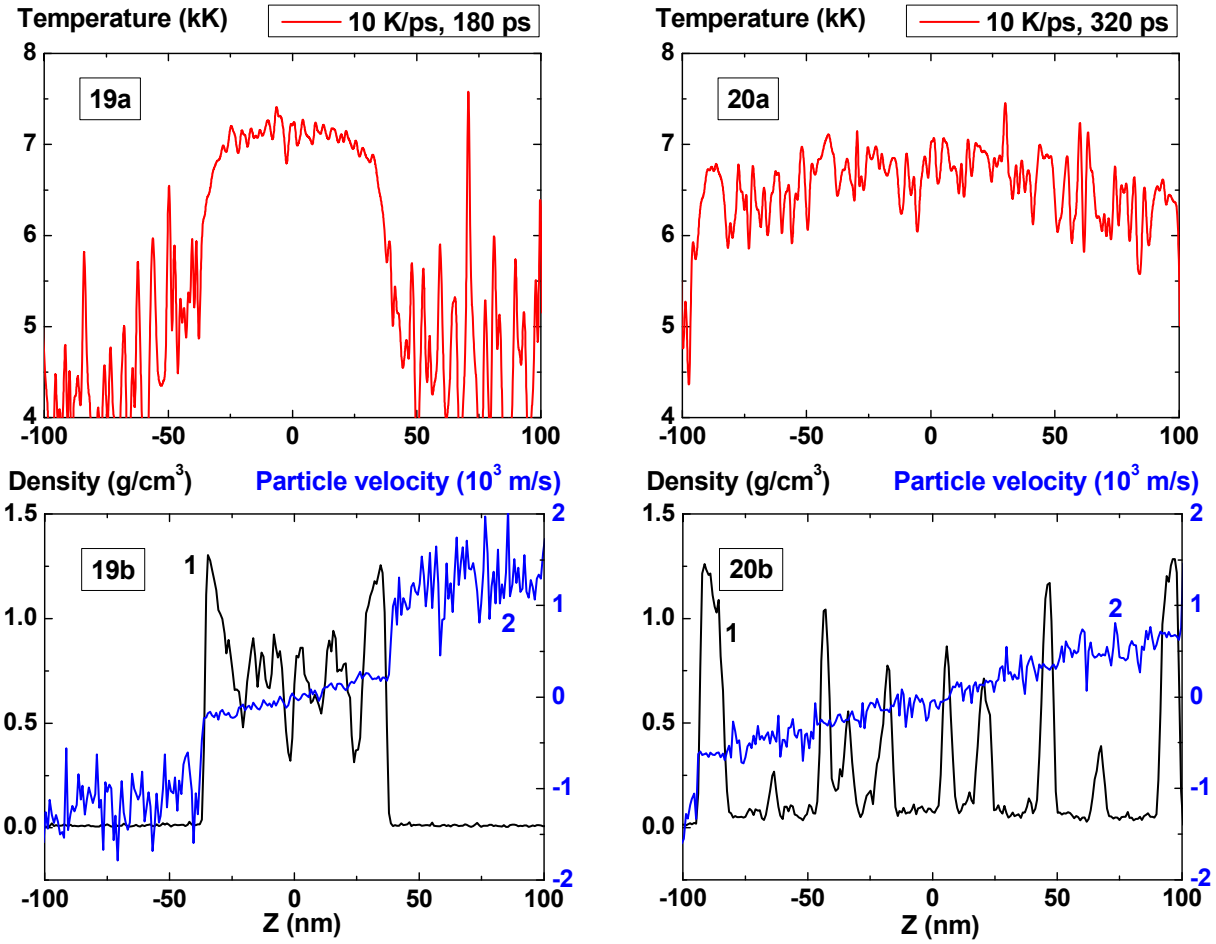

Figures 33-34: Spatial distributions of temperature (33a-34a), density (33b-34b, curve 1) and particle velocity(33b-34b, curve 2) through the film at moments 180, 320 ps during heating with 10 K/ps rate

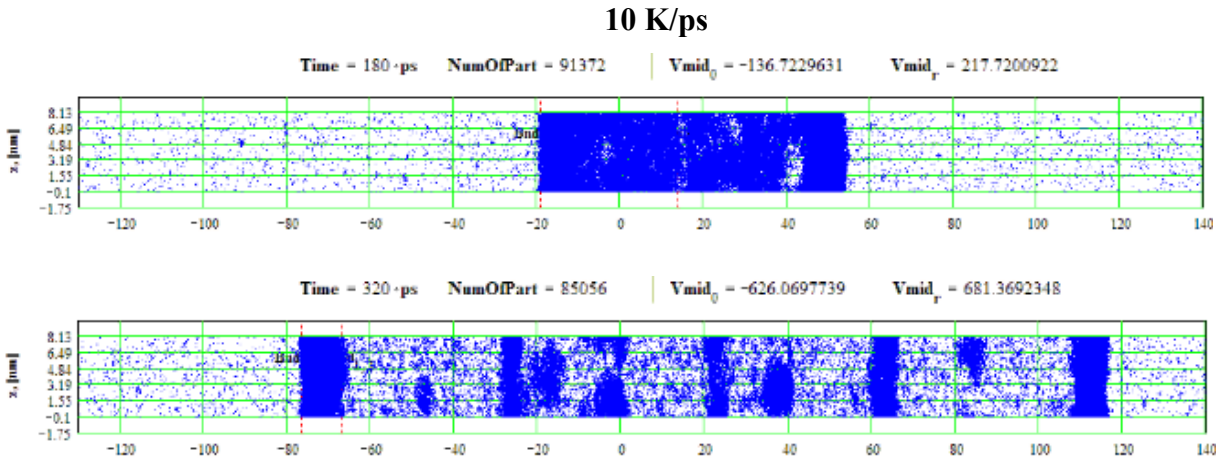

Figures 35-36: Spatial distributions of film particles at time moments 180, 320 ps during heating with 10 K/ps rate

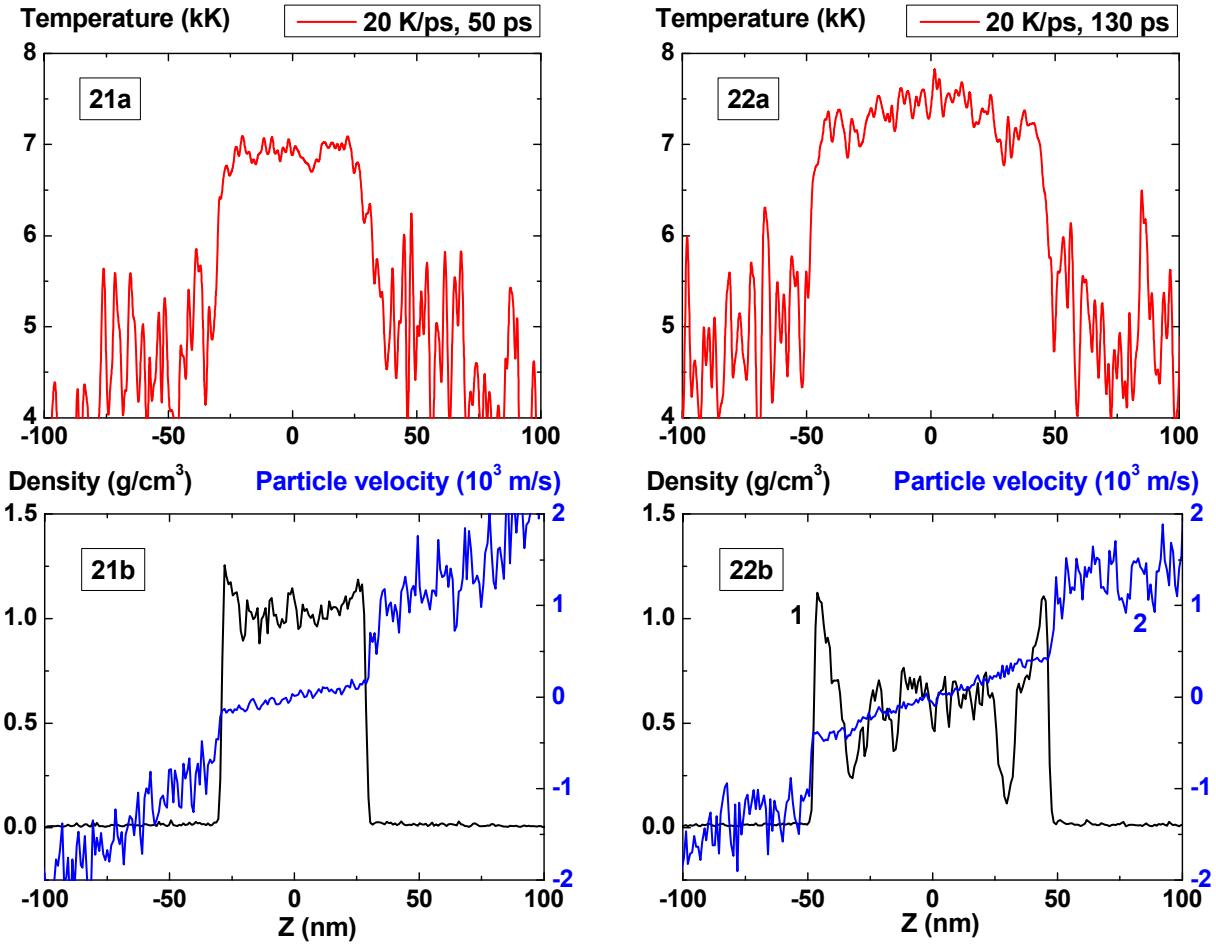

Fig.37-38: Spatial distributions of temperature (37a-38a), density (37b-38b, curve 1) and particle velocity (37b-38b, curve 2) through the film at moments 50, 130 ps during heating with 20 K/ps rate

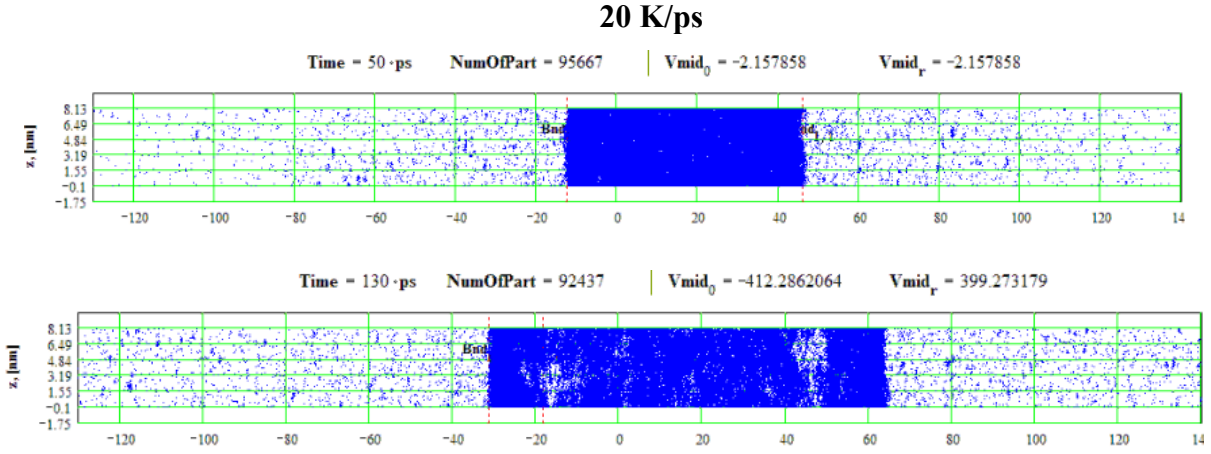

Figures 39-40: Spatial distributions of film particles at time moments 50, 130 ps during heating with 20 K/ps rate

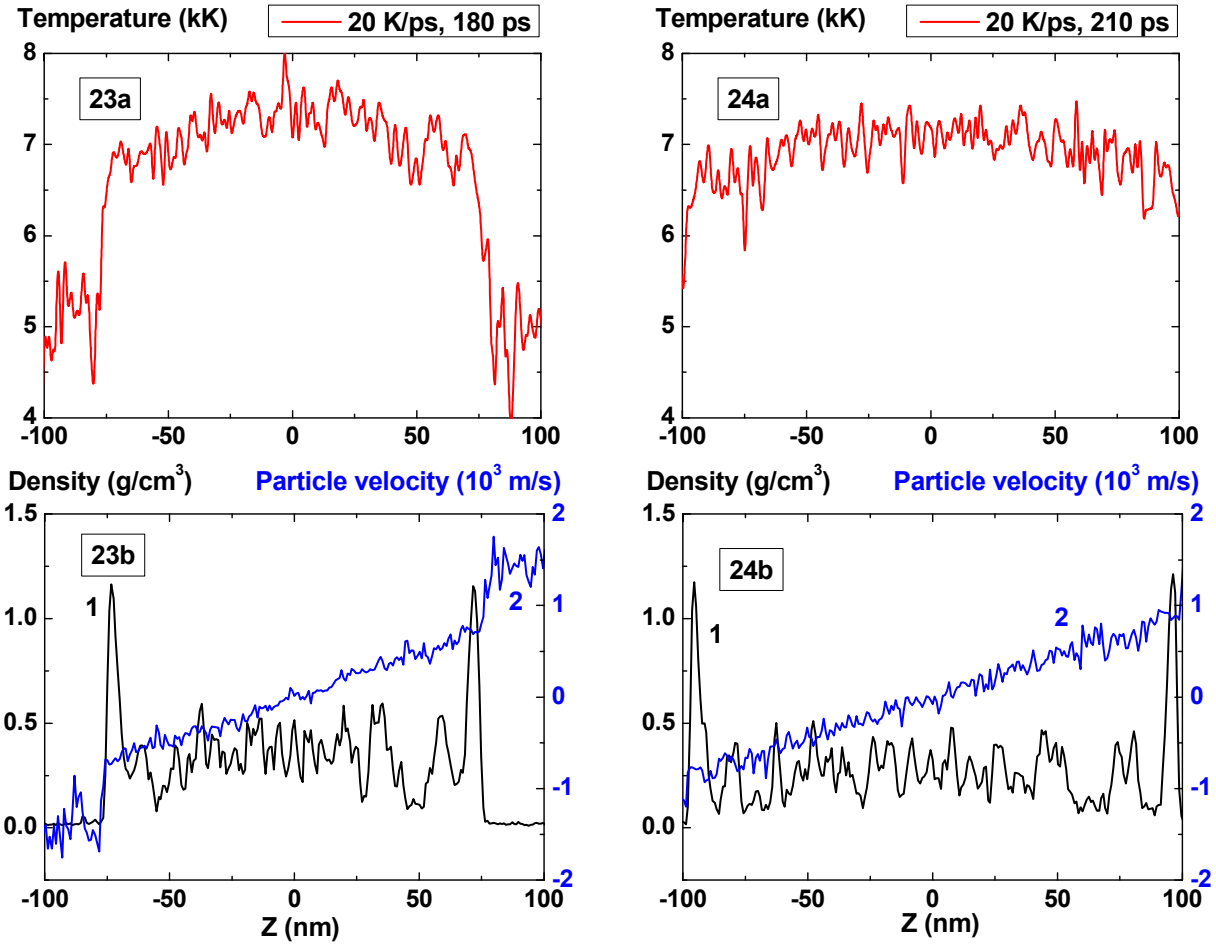

Figures 41-42: Spatial distributions of temperature (41a-42a), density (41b-42b, curve 1) and particle velocity (41b-42b, curve 2) through the film at moments 180, 210 ps during heating with 20 K/ps rate

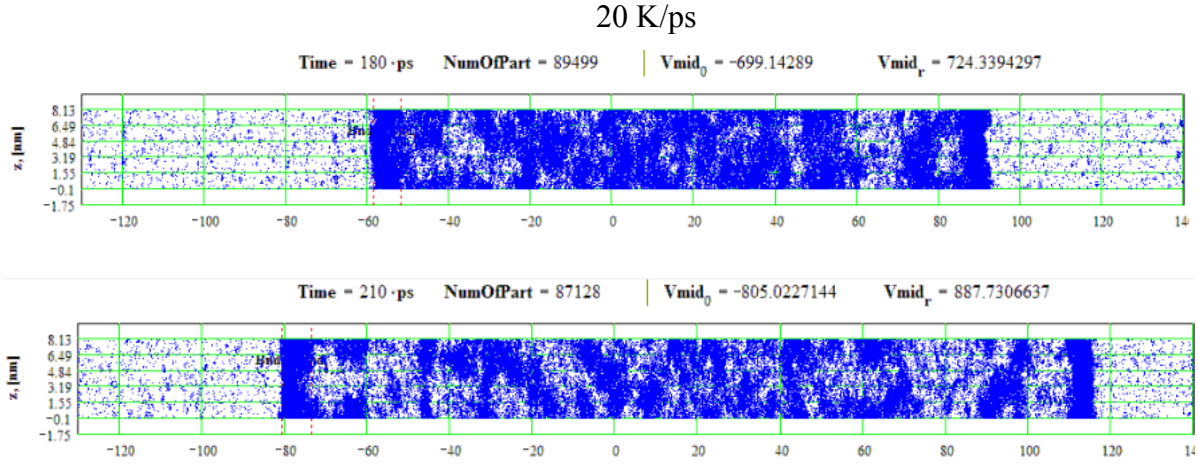

Figures 43-44: Spatial distributions of film particles at time moments 180, 210 ps during heating with 20 K/ps rate

It should be also noted that concave density distribution in the film becomes more wider during transition from 4 K/ps to 8 K/ps due to increase of large amplitude fluctuations number. As a result of such fluctuation widening the film decomposes onto six fragments (Fig. 21-28) instead of two (or three) at 4 K/ps.

Such film widening before its decomposition in fact means the decrease of its average density with temperature increase and this value of density as it was already mentioned before is lower than the equilibrium value due to metastable overheated state of the film. The decrease of density becomes more pronounced as it approaches the critical point. Such change of the film evolution parameters in this area is illustrated by data for the heating rate 10 K/ps presented at Fig. 29 - 36.

From the comparison of Fig. 25 and Fig. 33 that correspond to the same moment of time 180 ps from the start of the heating it is seen that the mean film thickness in the latter case is significantly larger than in the first one (over 30%) and is ~ 70 nm. In this case such evolution leads to film decomposition onto considerably more number of fragments than for heating rate 8 K/ps.

For 20 K/ps (Fig. 37-44) the density fluctuations amplitude becomes greater and instead of the collection of individual fragments of the condensed phase with steam interlayers (that can be seen at Fig. 34) one can observe vapor-drops mixture with diffuse inter-phase boundaries that is typical for the process of spinodal decomposition.

The evolution of film disintegration regimes at the stage of explosive boiling before spinodal decomposition is illustrated by 2D images presented at Fig. 39-40, 43-44. From this figures it is seen how the structure of the film fragments transforms when the heating rate changes from 4 to 20 K/ps. In this range the number of fragments grows and its vertical components cease to be explicitly evident, except two external fragments.

3.4 Rapid heating – regime of supercritical expansion

It is obvious that at further increase of the heating rate, beginning with some of the rate values, the density fluctuations amplitude in the process of film disintegration will decrease due to increase of the its number. Such regime in fact corresponds to expansion of dense non-ideal fluid because the stages described above (explosive boiling and spinodal decomposition) do not have time to develop in the process of rapid heating. Increasing of the internal pressure in the film, which does not have time to fully relax during heating also contributes to suppression of these stages.

In Fig. 45-52 the process of film disintegration at heating rate 40 K/ps is shown. If in the case of 10 K/ps the expansion stage becomes pronounced at times greater than 130 ps, while in the case of 40 K/ps this stage i.e. the increase of the film thickness due to density decrease and deviation of particles velocity distribution inside it from horizontal form is clear pronounced even at t = 40 ps. In this case (t = 40 ps) the film thickness h = 63 nm is significantly greater than its initial value h = 48 nm.

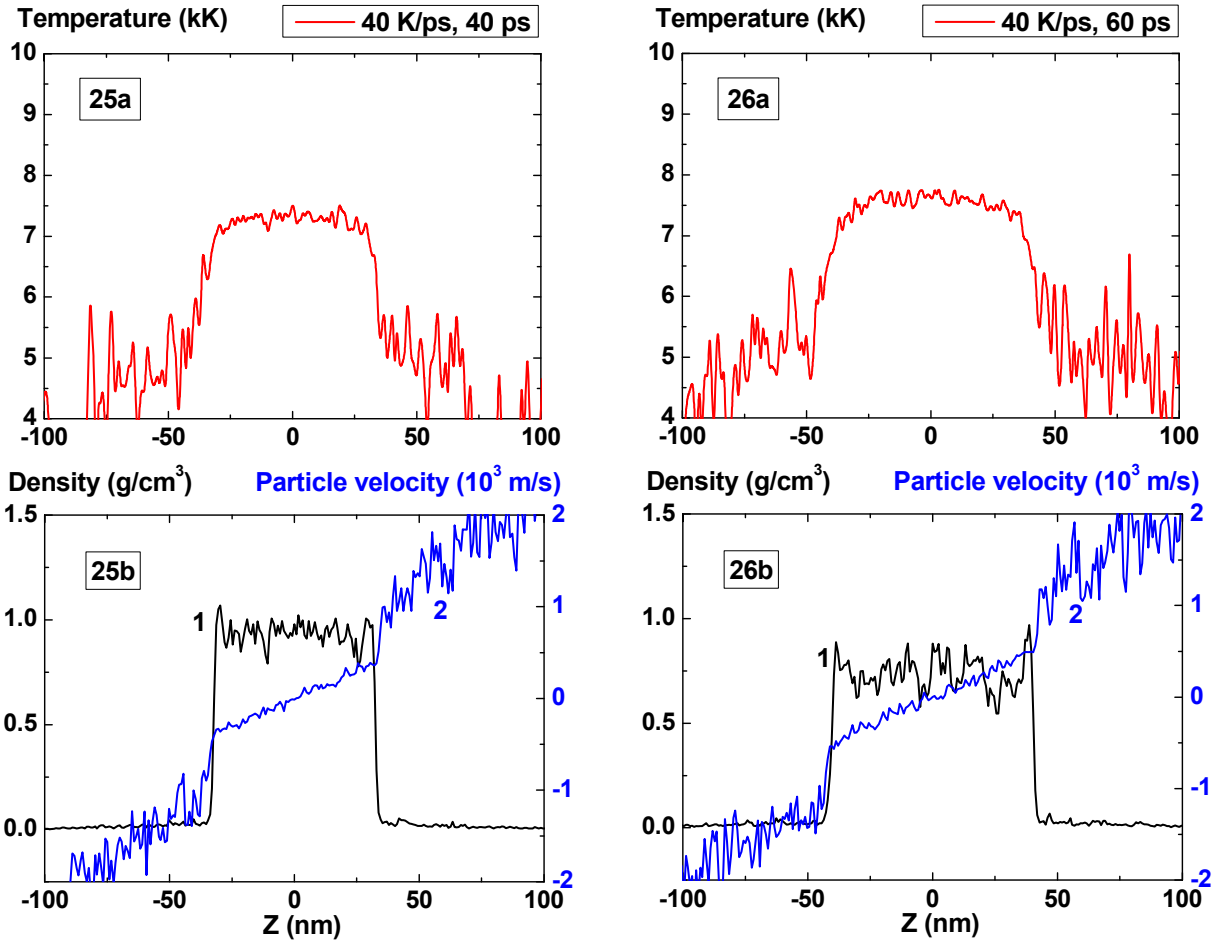

Figures 45-46: Spatial distributions of temperature (45a-46a), density (45b-46b, curve 1) and particle velocity (45b-46b, curve 2) through the film at moments 40, 60 ps during heating with 40 K/ps rate

40 K/ps

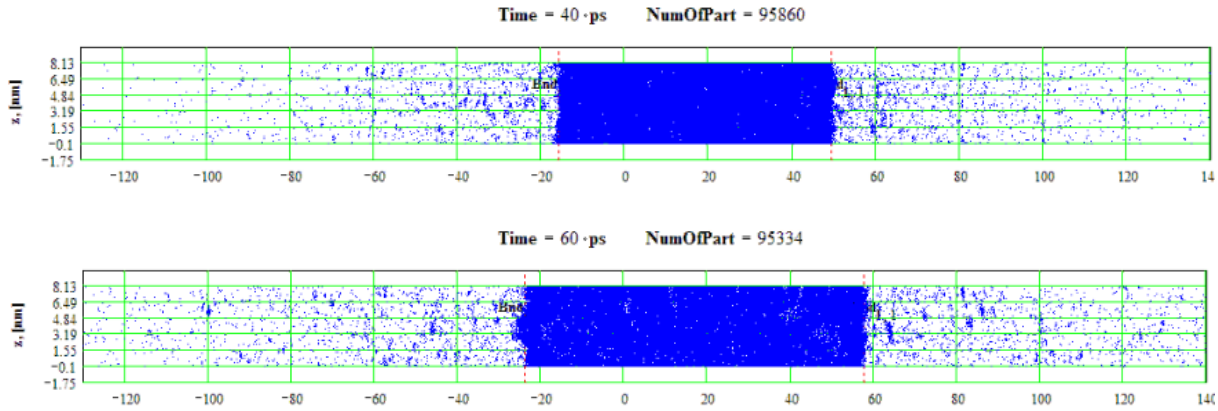

Figures 47-48: Spatial distributions of film particles at time moments 40, 60 ps during heating with 40 K/ps rate

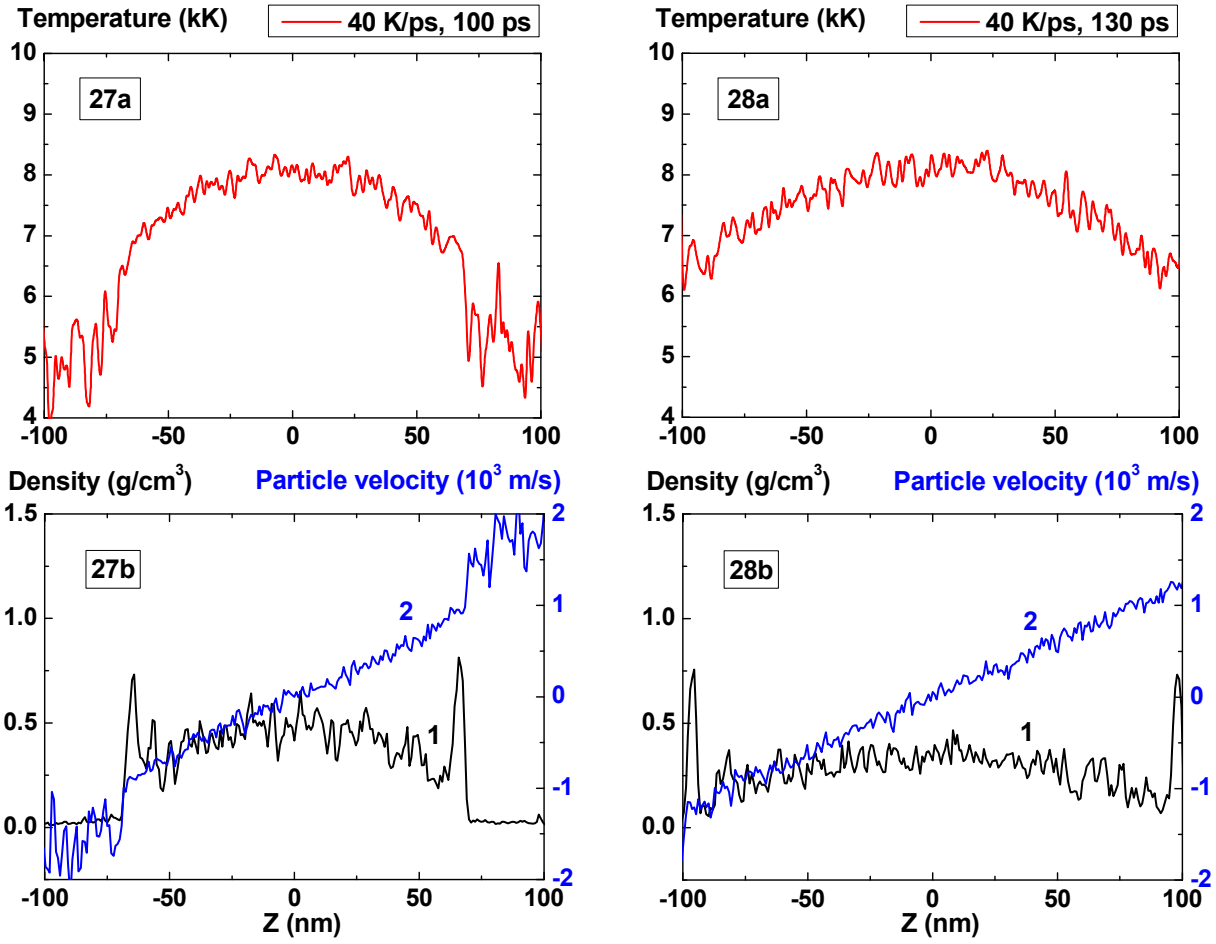

Figures 49-50: Spatial distributions of temperature (49a-50a), density (49b-50b, curve 1) and particle velocity (49b-50b, curve 2) through the film at moments 100, 130 ps during heating with 40 K/ps rate

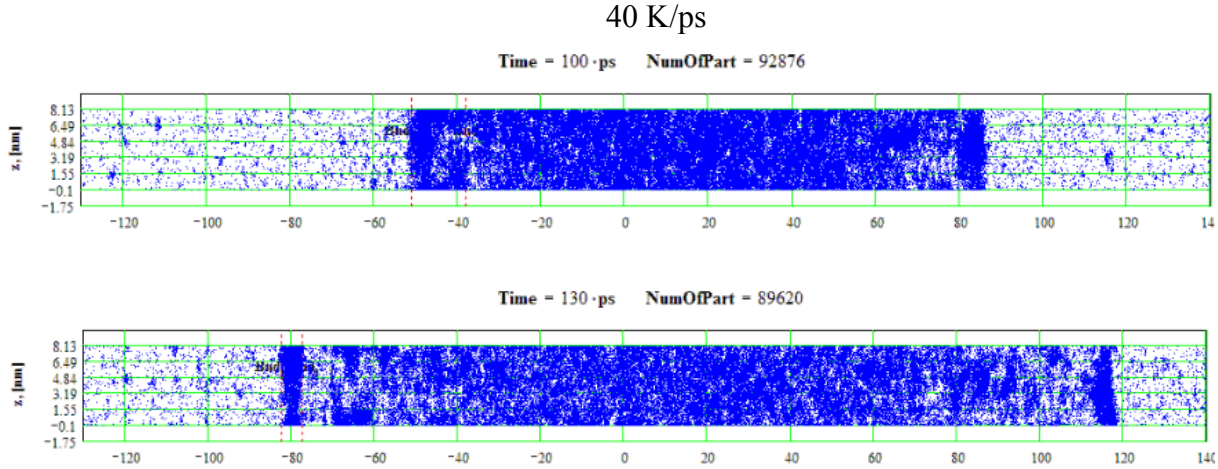

Figures 51-52: Spatial distributions of film particles at time moments 100, 130 ps during heating with 40 K/ps rate

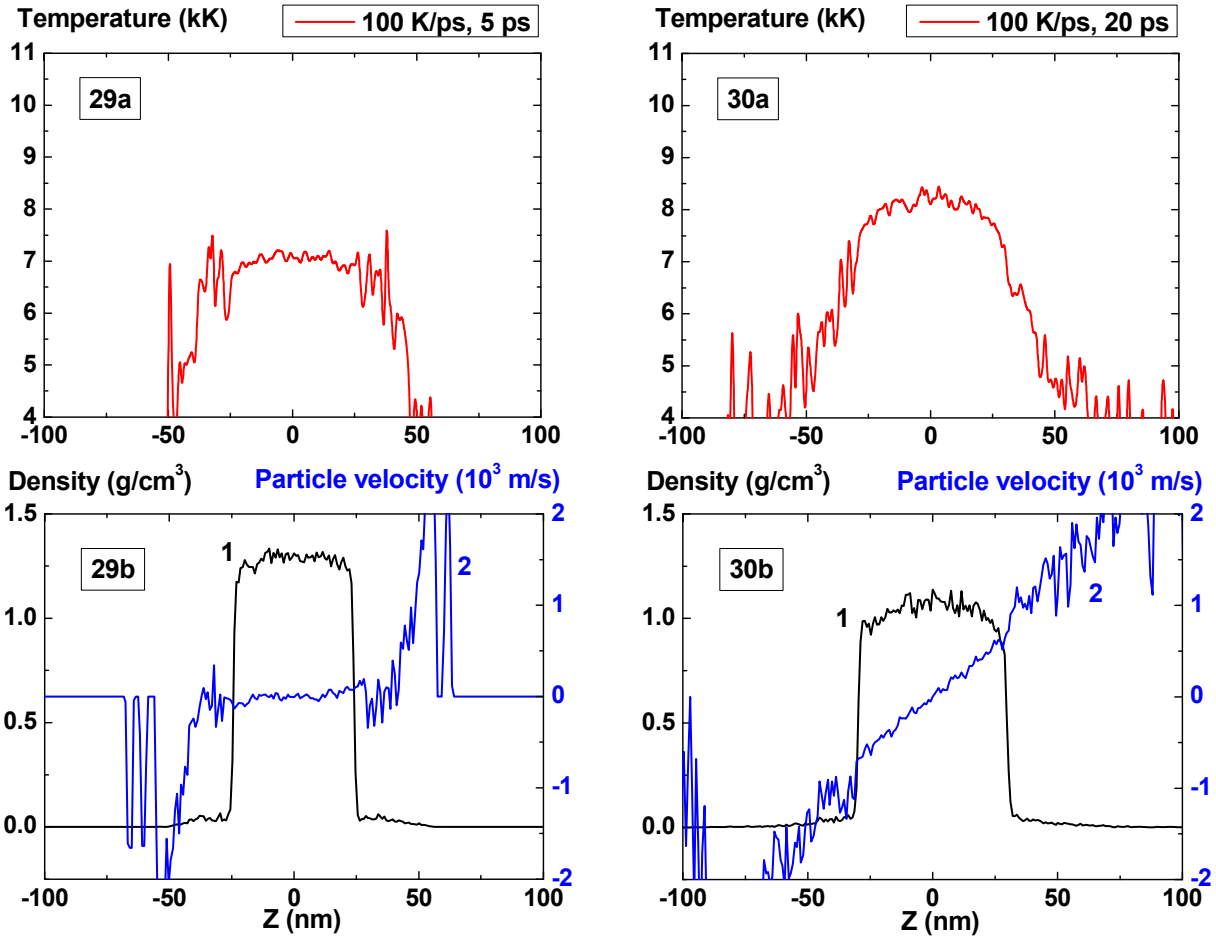

Figures 53-54: Spatial distributions of temperature (53a-54a), density (53b-54b, curve 1) and particle velocity (53b-54b, curve 2) through the film at moments 5, 20 ps during heating with 100 K/ps rate

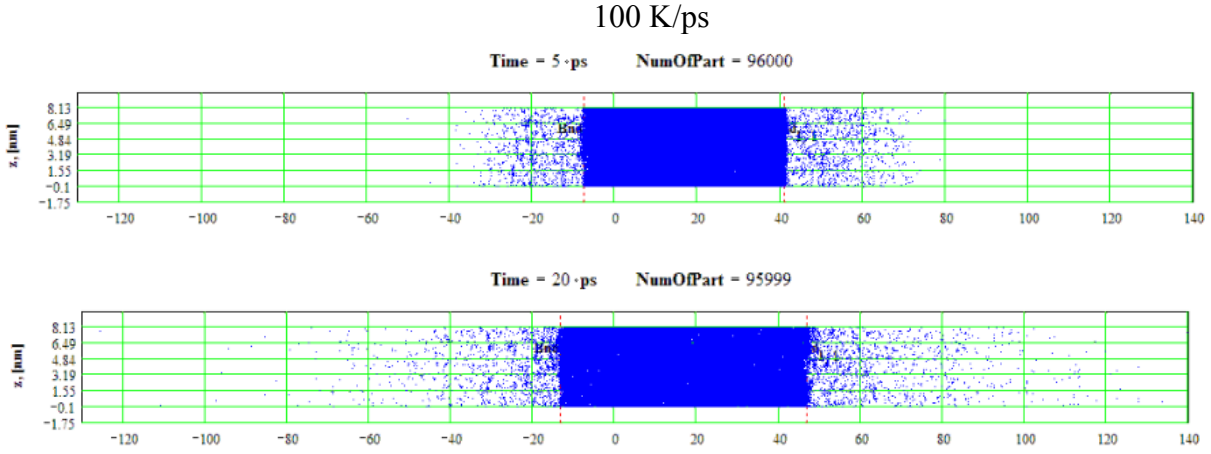

Figures 55-56: Spatial distributions of film particles at time moments 5, 20 ps during heating with 100 K/ps rate

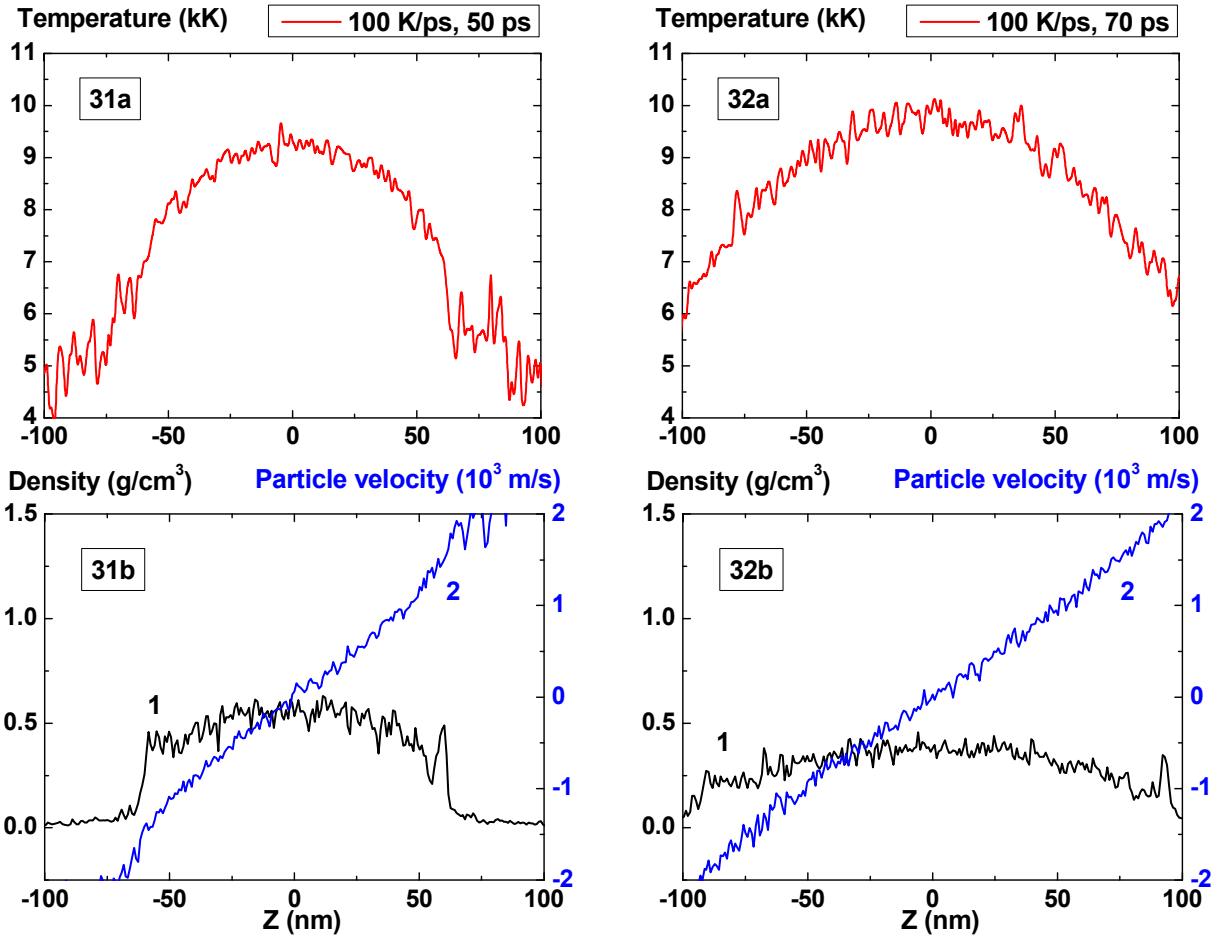

Figures 57-58: Spatial distributions of temperature (57a-58a), density (57b-58b, curve 1) and particle velocity (57b-58b, curve 2) through the film at moments 50, 70 ps during heating with 100 K/ps rate

100 K/ps

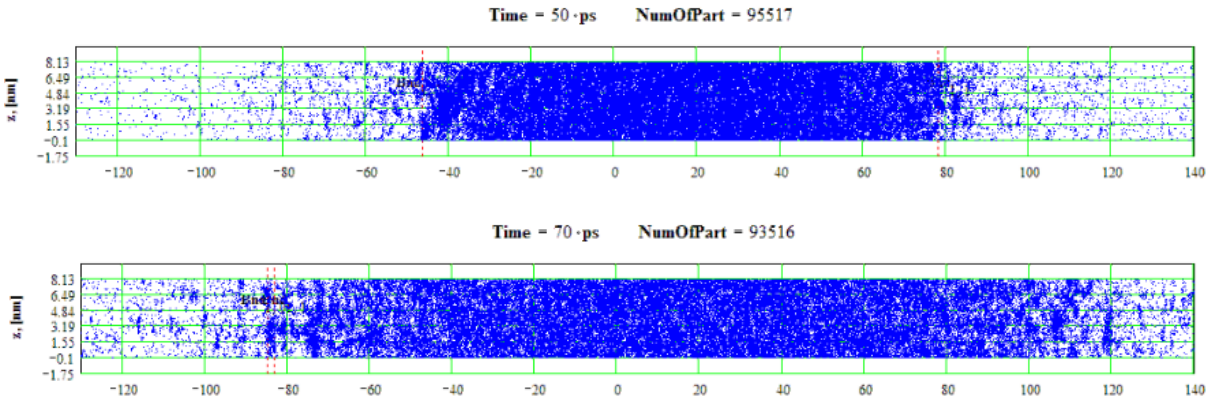

Figures 59-60: Spatial distributions of film particles at time moments 50, 70 ps during heating with 100 K/ps rate

In comparison with cases of 8, 10 and 20 K/ps heating rates the density fluctuations

are relatively small for all of the process except the stage where the mean density is smaller than 0.5 g/cm^3. At this final stage of expansion at the film borders the areas of high density are formed that are clear seen in Fig. 41 as a typical boundary peaks that is also observed in the range of smaller values of heating rate where the concave density profile inside the film is clearly pronounced. For 100 K/ps this boundary peaks are absent i.e. the influence of surface evaporation on density distribution in this regime of heating practically disappears. Such density behavior is also demonstrated in 2D images of density distribution (Fig. 55-56, 59-60).

For heating rates 40 and 100 K/ps density profile is not concave through all stage of heating. From the initial flat profile it converts to convex form which corresponds to the non-horizontal particle velocity profile of the film that is typical for its expansion state with overcritical temperature. It should be noted that the film temperature at heating rate 100 K/ps exceeds the critical one even at t = 5 ps and the pressure value in the film center at this moment is also greater than the critical value.

4. CONCLUSIONS

The results of the investigations allow to clearly distinguish three different regimes of film behavior.

For relatively slow heating – 2 K/ps from the initial state with equilibrium temperature 6400 K in the range of time up to 800 ps only surface evaporation of the film is observed that stabilize its temperature increase in maximum at level 6800 K.

The increase of the heating rate up to 4 K/ps leads to the development of the explosive (volume) boiling process with the formation of one cavity inside the film or two cavities that are divided by a thin layer of condensed phase.

The increase of the heating rate up to 8-10 K/ps is followed by increase of amplitude and number of density fluctuations before the start of rapid formation of vapor phase in it. Such change of the character of density fluctuations leads to the formation of multiple fragments in the process of disintegration the number of which rapidly grows with the increase of the heating rate.

Such behavior can be apparently connected with the reaching the spinodal decomposition regime that is observed at 20 K/ps when individual seeds of new phase are already hardly distinguished against the background of all of them. A distinctive feature of spinodal decomposition regime is also a smoothing of interfaces that are becoming less sharp than in the area of explosive boiling. The heating rate upper limit of this regime appears as a decrease in the amplitude of density fluctuations.

In the area of supercritical decomposition at heating rates of 40 and 100 K/ps density fluctuations are relatively small, which is consistent with the pattern of expansion of highly compressed non-ideal fluid, in which the two-phase state is almost never occur. The "edge effects" – peak density at the boundaries of the expanding cluster which are associated with the process of evaporation surface are exceptions.

A more detailed description of the above stages of non-equilibrium phase transformation at a uniform heating of the liquid film is possible using a quantitative analysis of the fluctuations behavior depending on the time, heating rates and other conditions of numerical simulation.

The work was partially supported by RFBR grant №13-02-01129a, №13-07-00597, № 12-07-00436.

REFERENCES

[1] L.V. Zhigilei, Z. Lin and D.S. Ivanov, "Atomistic modeling of short pulse laser ablation of metals: connections between melting, spallation, and phase explosion", *J. Phys. Chem. C*, **113**, 11892-11906 (2009).

[2] P. Lorazo, L.J. Lewis, M. Meunier, "Thermodynamic pathways to melting, ablation, and solidification in absorbing solids under pulsed laser irradiation", *Physical Review B*, **73**, 134108 (2006).

[3] S.I. Anisimov, V.V. Zhakhovskii, N.A. Inogamov, K. Nishihara, A.M. Oparin and Yu.V. Petrov, "Destruction of a solid film under the action of ultrashort laser pulse", *JETP Lett.*, **77**, 606-610 (2003).

[4] G.E. Norman, S.V. Strarikov and V.V. Stegailov, "Atomistic simulation of laser ablation of gold: effect of pressure relaxation", *JETP*, **114**, 792-800 (2012).

[5] T.H. Yang and C. Pan, "Molecular dynamics simulation of a thin water layer evaporation and evaporation coefficient", *Intern. Journ. of Heat and Mass Transfer*, **48**, 3516-3526 (2005).

[6] V.I. Mazhukin and A.V. Shapranov, Molekuliarno-dinamicheskoe modelirovanie processov nagreva i plavleniia metallov. I. Model' i Vychislinel'nyi algoritm, *M.V. Keldysh Institute of Applied Mathematics of RAS, Preprint* **31** (2012) (In Russian).

[7] M.S. Daw amd M.I. Baskes, "Embedded-atom method: Derivation and application to impurities and other defects in metals", *Phys. Rev. B*, **29**, 6443-6453 (1984).

[8] S.M. Foiles, M.I. Baskes and M.S. Daw, "Embedded-atom-method functions for the fcc metals Cu, Ag, Au, Ni, Pd, Pt, and their alloys", *Phys. Rev. B*, **33**, 7983-7991, (1986).

[9] V.V. Zhakhovskii, N.A. Inogamov, Yu.V. Petrov, S.I. Ashitkov and K. Nishihara. "Two-temperature relaxation and melting after absorption of femtosecond laser pulse", *Appl. Surf. Sci.*, **255**, 9592-9596 (2009).

[10] V.I. Mazhukin, A.V. Shapranov, Molekuliarno-dinamicheskoe modelirovanie processov nagreva i plavleniia metallov. II. Vychislinel'nyi experiment. *M.V. Keldysh Institute of Applied Mathematics of RAS, Preprint,* **32** (2012) (in Russian).

[11] V.I. Mazhukin, A.V. Shapranov, V.E. Perezhigin, "Mathematical modeling of thermophysical properties, heating and melting processes of metal with the molecular dynamics method", *Mathematica Montisnigri*, **24**, 47–66, (2012) (In Russian).

[12] L. Verlet, "Computer "experiments" on classical fluids. I. Thermodynamical properties of Lennard-Jones molecules", *Phys. Rev.*, **159**, 98-103, (1967).

[13] V.P. Skripov, *Metastable liquids*, Wiley (1974).

[14] B.J. Garrison, T.E. Itina and L.V. Zhigiley, "Limit of overheating and the threshold behaviour in laser ablation", Phys. Rev. E, **68**, 041501 (2003).

Received June 20, 2013